Key Points:
- Emissivity and reflectance spectroscopies used for first time on vent samples
- Spectroscopies corroborated petrography, XRD, and elemental analyses
- Conditions within metal-sulfide edifices may promote anaerobic metabolisms

Correspondence to:
J. F. Holden,
jholden@microbio.umass.edu

Linkages between mineralogy, fluid chemistry, and microbial communities within hydrothermal chimneys from the Endeavour Segment, Juan de Fuca Ridge

T. J. Lin[1], H. C. Ver Eecke[1], E. A. Breves[2], M. D. Dyar[2], J. W. Jamieson[3,4], M. D. Hannington[3], H. Dahle[5], J. L. Bishop[6], M. D. Lane[7], D. A. Butterfield[8], D. S. Kelley[9], M. D. Lilley[9], J. A. Baross[9], and J. F. Holden[1]

[1]Department of Microbiology, University of Massachusetts, Amherst, Massachusetts, USA, [2]Department of Astronomy, Mount Holyoke College, South Hadley, Massachusetts, USA, [3]Department of Earth Sciences, University of Ottawa, Ottawa, Ontario, Canada, [4]GEOMAR, Helmholtz Centre for Ocean Research, Kiel, Germany, [5]Department of Biology, Centre for Geobiology, University of Bergen, Bergen, Norway, [6]SETI Institute/NASA Ames Research Center, Moffett Field, California, USA, [7]Planetary Science Institute, Tucson, Arizona, USA, [8]Joint Institute for the Study of the Atmosphere and Ocean, University of Washington and NOAA-PMEL, Seattle, Washington, USA, [9]School of Oceanography, University of Washington, Seattle, Washington, USA

Abstract Rock and fluid samples were collected from three hydrothermal chimneys at the Endeavour Segment, Juan de Fuca Ridge to evaluate linkages among mineralogy, fluid chemistry, and microbial community composition within the chimneys. Mössbauer, midinfrared thermal emission, and visible-near infrared spectroscopies were utilized for the first time to characterize vent mineralogy, in addition to thin-section petrography, X-ray diffraction, and elemental analyses. A 282°C venting chimney from the Bastille edifice was composed primarily of sulfide minerals such as chalcopyrite, marcasite, and sphalerite. In contrast, samples from a 300°C venting chimney from the Dante edifice and a 321°C venting chimney from the Hot Harold edifice contained a high abundance of the sulfate mineral anhydrite. Geochemical modeling of mixed vent fluids suggested the oxic-anoxic transition zone was above 100°C at all three vents, and that the thermodynamic energy available for autotrophic microbial redox reactions favored aerobic sulfide and methane oxidation. As predicted, microbes within the Dante and Hot Harold chimneys were most closely related to mesophilic and thermophilic aerobes of the *Betaproteobacteria* and *Gammaproteobacteria* and sulfide-oxidizing autotrophic *Epsilonproteobacteria*. However, most of the microbes within the Bastille chimney were most closely related to mesophilic and thermophilic anaerobes of the *Deltaproteobacteria*, especially sulfate reducers, and anaerobic hyperthermophilic archaea. The predominance of anaerobes in the Bastille chimney indicated that other environmental factors promote anoxic conditions. Possibilities include the maturity or fluid flow characteristics of the chimney, abiotic Fe^{2+} and S^{2-} oxidation in the vent fluids, or O_2 depletion by aerobic respiration on the chimney outer wall.

1. Introduction

Hydrothermal vent fluids form as subseafloor seawater exchanges ions during reactions with subsurface rocks. Fluid-mineral reactions result in the loss of some dissolved chemical and volatile components (e.g., O_2, Mg^{2+}, SO_4^{2-}) and gain in others (e.g., H_2, CH_4, CO_2, H_2S, reduced metals, SiO_2) at progressively higher temperatures as modified seawater migrates deeper into the oceanic crust [*Kelley et al.*, 2002; *Von Damm*, 1995]. Submarine hydrothermal chimneys form when metal sulfides precipitate from hot vent fluid upon mixing with cold seawater and through conductive cooling [*Goldfarb et al.*, 1983; *Haymon*, 1983; *Kelley et al.*, 2002; *Tivey*, 1995]. Precipitation of anhydrite ($CaSO_4$) occurs during heating of seawater above 150°C, while barite ($BaSO_4$) precipitation occurs when seawater mixes with hydrothermal fluid [*Kristall et al.*, 2006; *Mills and Elderfield*, 1995]. Chimney walls are commonly porous and permit the exchange of hydrothermal fluid and seawater through much of their interiors, creating temperature and chemical gradients between end-member, hot hydrothermal fluids emitted from the interior and cold seawater [*Kristall et al.*, 2006; *Tivey and Singh*, 1997; *Zhu et al.*, 2007]. Fracturing of chimney walls also allows ingress of seawater far into the chimney interiors, and outpouring of hot hydrothermal fluids [*Kelley et al.*, 2002]. The resulting chemical disequilibria between the reduced chemical species in the hydrothermal fluid and the relatively oxidized
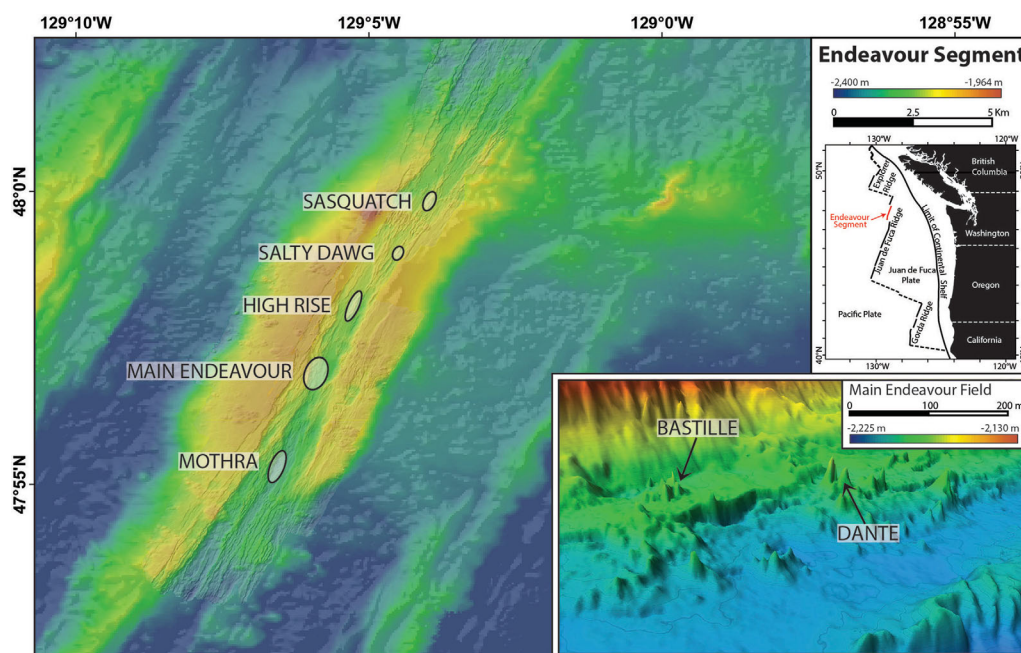
Figure 1. Bathymetric map of the Endeavour Segment, showing the locations of the main active vent fields. Inset image shows the locations of the Bastille and Dante edifices (at 2× vertical exaggeration) within the Main Endeavour Field. Regional bathymetry (gridded at 50 m) from *Kelley et al.* [2002], and high-resolution bathymetry of the axial valley and inset image (gridded at m) from *Clague et al.* [2008].

surrounding environment are used by microbes living within and on the exterior of hydrothermal chimneys for their growth [*McCollom and Shock*, 1997; *Tivey*, 2004]. This study examines the interrelationships among mineral assemblages, hydrothermal fluid chemistry, and microbial communities within hydrothermal chimneys from the Endeavour Segment, Juan de Fuca Ridge with varying morphologies and mineral compositions.

Hydrothermal venting along the Endeavour Segment (Figure 1) results in the formation of sulfide-sulfate-silica deposits that rise up to 45 m above the seafloor and reach 50 m across [*Delaney et al.*, 1992; *Kelley et al.*, 2002, 2012, 2014; *Robigou et al.*, 1993]. The mineralogical-permeability relationships of the chimneys are highly variable depending on the "maturity" of the edifices [*Delaney et al.*, 1992; *Kelley et al.*, 2002; *Kristall et al.*, 2006, 2011; *Tivey and Delaney*, 1986; *Tivey et al.*, 1999; *Zhu et al.*, 2007]. Young chimneys that are typically near the summits of the massive structures are characterized by highly friable growths of intermixed fine-grained sulfide and anhydrite. In contrast, a general cross section through a mature Endeavour chimney includes an outer sulfide zone hosting variable amounts of sulfide and sulfate minerals enclosed by amorphous silica, as well as variably fossilized tube worms and iron hydroxide phases [*Kelley et al.*, 2002; *Kristall et al.*, 2006; *Tivey and Delaney*, 1986; *Tivey et al.*, 1999]. The inner portions of the chimneys are marked by anastomosing, discontinuous networks of channels through a sponge-like matrix of amorphous silica and sulfide phases with lesser sulfate, and clay minerals resulting from seawater ingress, outflow of warm fluids, and conductive cooling [*Kristall et al.*, 2006, 2011; *Tivey and Delaney*, 1986]. The highest temperature inner conduits are typically lined with chalcopyrite [*Kelley et al.*, 2002, 2014].

Hydrothermal fluids at the Endeavour Segment are relatively methane-rich and ammonia-rich for a sediment-free, basaltic environment. It is thought that the unusual methane and ammonia concentrations result from decomposition of sediments that were overrun by lava flows [*Lilley et al.*, 1993]. The elevated ammonia concentrations cause higher than normal fluid pH due to ammonia-ammonium buffering [*Butterfield et al.*, 1994; *Lilley et al.*, 1993]. As a result, deposition of sulfide minerals, amorphous silica, and clay phases is enhanced [*Kristall et al.*, 2006; *Tivey et al.*, 1999]. This, coupled with the presence of magma chambers that underlie all of the main hydrothermal fields, elevated seismic activity, and venting that persists for hundreds to thousands of years leads to the formation of large edifices [*Jamieson et al.*, 2013; *Kelley et al.*, 2012; *Kristall et al.*, 2006; *Tivey and Delaney*, 1986; *Tivey et al.*, 1999].

Studies that relate the mineralogy of hydrothermal chimneys to their endemic microbial community compositions are limited for Endeavour [*Schrenk et al.*, 2003; *Zhou et al.*, 2009] and elsewhere [e.g., *Kormas et al.*, 2006; *Olins et al.*, 2013; *Pagé et al.*, 2008; *Takai et al.*, 2001]. Generally, they show that the cooler exterior regions of hydrothermal vents contain a mix of bacteria and archaea, with a shift to predominantly archaea toward the hotter interior regions [*Hedrick et al.*, 1992; *Pagé et al.*, 2008; *Schrenk et al.*, 2003]. The archaea in these hotter regions are primarily hyperthermophiles (i.e., organisms with optimal growth above 80°C) typically belonging to the taxonomic orders *Thermococcales*, *Desulfurococcales*, *Methanococcales*, and *Archaeoglobales* [*Kormas et al.*, 2006; *Pagé et al.*, 2008; *Schrenk et al.*, 2003; *Takai et al.*, 2001; *Zhou et al.*, 2009]. *Epsilonproteobacteria*, typically related to autotrophic sulfur oxidizers, are ubiquitous in cooler regions [*Kormas et al.*, 2006; *Olins et al.*, 2013; *Zhou et al.*, 2009]. Hydrothermal vent microbes are found in mineral deposits that range from those dominated by metal sulfide and amorphous silicate [*Kormas et al.*, 2006; *Schrenk et al.*, 2003; *Zhou et al.*, 2009] to those composed predominantly of anhydrite [*Frank et al.*, 2013; *Olins et al.*, 2013; *Pagé et al.*, 2008].

The goal of this study was to improve our understanding of the mineral and microbial composition of habitable zones within the walls of active hydrothermal mineral deposits and the relationships among minerals, hydrothermal fluids, and microbes. Mineral spectroscopic techniques (Mössbauer, thermal emission, and visible-near infrared (VNIR)) were used for the first time to characterize the mineralogy and microbial pigments (e.g., chlorophyll) of chimney interiors in tandem with more common techniques for mineral characterization (thin-section petrography, elemental analyses, and X-ray diffraction). If successful, these spectroscopic techniques would provide the means for future rapid, nondestructive shipboard analysis of samples. Emphasis was placed on characterizing the friable, fine-grained, and very porous material in the midwall of these chimneys, which was previously shown to host anaerobic, hyperthermophilic microorganisms [*Ver Eecke et al.*, 2009, 2012]. The microbial community associated with this interior mineral matrix was determined through molecular analysis of the 16S rRNA genes present and by culture-dependent abundance analysis for various metabolic types of hyperthermophiles. Calculations of Gibbs energies at different mixing ratios of hydrothermal fluids and seawater were made for various autotrophic redox reactions to estimate microbial growth potential.

Three actively venting and morphologically distinct hydrothermal chimneys and their associated fluids were sampled in 2008 from the Main Endeavour and Mothra hydrothermal fields on the Endeavour Segment, Juan de Fuca Ridge (Figure 1). This study demonstrates that mineral spectroscopic techniques are effective at identifying minerals and biological pigments within vent chimneys, and could be used for rapid shipboard analyses prior to subsampling. In contrast to previous predictions [e.g., *Amend et al.*, 2011; *McCollom and Shock*, 1997], it also suggests that aerobic versus anaerobic microbial metabolisms are influenced by factors other than simply conservative mixing of hydrothermal fluid and seawater such as fluid flow characteristics and maturity of the chimney.

2. Geologic Setting

The Juan de Fuca Ridge is an intermediate-spreading-rate mid-ocean ridge that strikes 020° and forms the boundary between the Pacific and Juan de Fuca tectonic plates in the northeastern Pacific Ocean (Figure 1). The Endeavour Segment extends ∼90 km in length and is bounded to the north by Middle Valley and to the south by the Cobb Segment [*Karsten et al.*, 1986]. It is marked by an axial valley 500–1000 m wide with walls up to 200 m in height, with water depths ranging from ∼2050 m in the central portion of the segment to maximum depths >2700 m to the north and south of the central high [*Delaney et al.*, 1992; *Kelley et al.*, 2012, 2014]. Within the central 15 km of the axial valley, there are five major active high-temperature hydrothermal fields, each separated by ∼2–3 km [*Kelley et al.*, 2002, 2012]. The fields host a myriad of focused-flow vent sites with diffuse-flow vent sites within and far-afield from the high-temperature fields [*Delaney et al.*, 1992; *Kelley et al.*, 2012; *Robigou et al.*, 1993]. From the north to the south these fields are Sasquatch, Salty Dawg, High Rise, Main Endeavour, and Mothra (Figure 1).

The fields are underlain by a series of discontinuous seismic reflectors 2.2–3.3 km below the seafloor that are interpreted to reflect the tops of magma chambers [*Carbotte et al.*, 2012; *Van Ark et al.*, 2007]. The valley is strongly tectonized and no seafloor eruptions have been documented since studies first started here in the 1980s [*Clague et al.*, 2014; *Delaney et al.*, 1992; *Kelley et al.*, 2002, 2012, 2014]. Until 2006, the area was

marked by intense low magnitude, seismic activity. Seismic swarms within the axial valley in 1999–2000, 2003–2004, and 2005 were attributed to shallow diking events that altered hydrothermal vent fluid temperatures, fluxes, and chemistries, indicating that volcanic and magmatic processes are important influences along the segment [*Bohnenstiehl et al.*, 2004; *Davis et al.*, 2001; *Hooft et al.*, 2010; *Kelley et al.*, 2012; *Lilley et al.*, 2003; *Proskurowski et al.*, 2004; *Seyfried et al.*, 2003; *Weekly et al.*, 2013; *Wilcock et al.*, 2009]. A dramatic decrease in seismic activity since 2005 is interpreted to reflect the end of a noneruptive spreading event that lasted 6 years [*Weekly et al.*, 2013].

There are over 800 individual active or extinct hydrothermal chimneys within the central 15 km portion of the Endeavour Segment [*Clague et al.*, 2008; *Jamieson et al.*, 2014]. Most of the active chimneys are located within the five major hydrothermal fields. Hydrothermal venting has been ongoing at Sasquatch, High Rise, and Main Endeavour for at least 1450, 850, and 2300 years, respectively, based on ^{226}Ra/Ba dating of hydrothermal barite [*Jamieson et al.*, 2013]. Focused, high-temperature venting in the High Rise, MEF, and Mothra fields typically originates from several point sources atop large, steep-sided hydrothermal edifices [*Delaney et al.*, 1992; *Kelley et al.*, 2002, 2012; *Robigou et al.*, 1993]. High-temperature flow also issues from horizontal outcrops, or "flanges," that pool high-temperature hydrothermal fluids beneath them. Overflowing of pools by the buoyant hydrothermal fluids results in the egress of fluids upward around the flange edges [*Delaney et al.*, 1992; *Kelley et al.*, 2001, *Robigou et al.*, 1993; *Tivey and Delaney*, 1986; *Tivey et al.*, 1999]. The outer walls of the chimneys are typically awash in variable mixtures of high-temperature hydrothermal fluids and seawater [*Delaney et al.*, 1992; *Kelley et al.*, 2001; *Kristall et al.*, 2006; *Robigou et al.*, 1993].

3. Materials and Methods

3.1. Sample Collection

Three actively venting hydrothermal chimneys and corresponding hydrothermal fluids were sampled in 2008 using the deep-sea research submersible *Alvin*, operating from the R/V *Atlantis*. Samples were collected from the Bastille and Dante edifices in the MEF at depths of 2193 m and 2186 m, respectively; and from the Hot Harold edifice in the Faulty Towers hydrothermal complex in the Mothra Field at a depth of 2271 m. Sampling focused on ∼0.5 m tall actively venting chimneys that could be readily recovered by *Alvin*. Prior to sampling, the chimneys were photographed. The maximum temperature of the exiting hydrothermal fluid was measured using the submersible's high-temperature probe, either prior to or after removal of the chimneys. The first chimney sampled from the Bastille edifice in the Main Endeavour Field was a black smoker venting 282°C fluid. The second chimney from the Dante edifice in the MEF was a bulbous "beehive" chimney venting 300°C clear hydrothermal fluid. The third chimney, venting 321°C fluid from the Hot Harold edifice in the Mothra hydrothermal field, was from a "candelabra" proto-chimney formed atop a vigorously venting edifice. The chimneys were broken off near their bases using the submersible's manipulators and placed into PVC boxes with sealable lids in the front basket of the submersible to minimize damage to the chimney during surface recovery. Subsequent to chimney sampling, hydrothermal fluids were collected using titanium syringe major samplers, the Hydrothermal Fluid and Particle Sampler (HFPS), and titanium gas-tight samplers [*Butterfield et al.*, 1997; *Edmond et al.*, 1992].

Once shipboard, the recovered chimney material was photographed (Figures 2–4). Larger fragments were selected and cracked open while exposed to air using a hammer and chisel that were sterilized with 95% (v/v) ethanol and by pulling the pieces apart without direct contact with the interior. Once exposed, 35–50 g of the friable, porous material in the chimney wall between the central chalcopyrite-lined fluid conduit (if present) and the harder exterior were removed using a sterile spoon and placed into sterile plastic dishes. This material was mixed by hand and divided into three portions. The first portion (10–15 g) was added to sterile, anoxic artificial seawater, sealed in a serum bottle with a rubber stopper, flushed with N$_2$ gas, and reduced with 0.025% (w/v) each of cysteine-HCl and Na$_2$S·9H$_2$O as previously described [*Ver Eecke et al.*, 2009, 2012]. This was used to inoculate media for growth of hyperthermophilic anaerobic microorganisms (see section 3.6). The second portion (15–20 g) was placed into a sterile 50 mL Falcon tube and frozen immediately at −80°C for land-based DNA extractions (see section 3.6). The third portion (10–15 g) was immediately air dried and used for land-based mineral spectroscopy and X-ray diffraction (XRD) analyses (see section 3.2). Representative whole samples (i.e., those with intact interiors) adjoining those sampled as described above were set aside for petrography and elemental analysis (see section 3.3). These samples
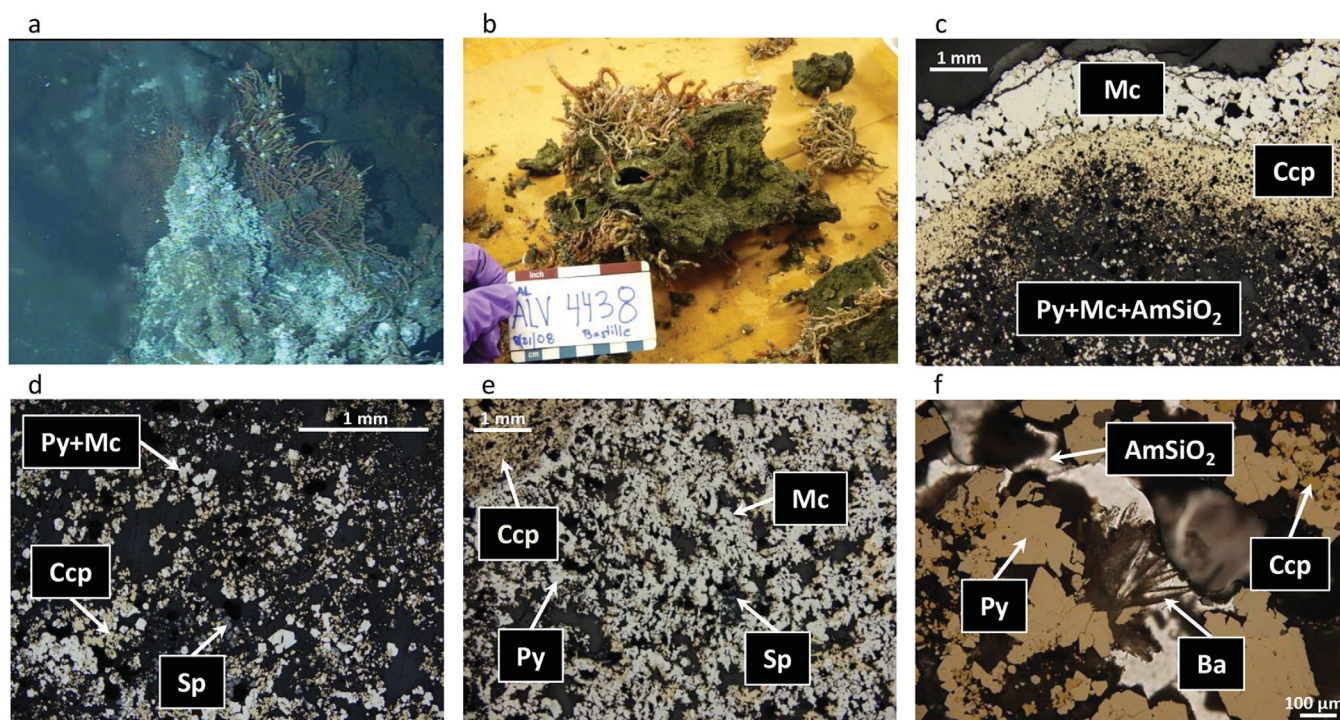
Figure 2. Bastille chimney sample. (a) Hydrothermal chimney actively venting 282°C fluid as seen on the seafloor prior to collection. (b) The hydrothermal chimney fragments as seen on board ship prior to subsampling. (c) Reflected light photomicrograph (RLP) showing concentric sulfide layering of marcasite (Mc) and chalcopyrite (Ccp) lining an open conduit (top), and a gradational shift to a typical lower temperature porous assemblage of pyrite (Py), marcasite, and amorphous silica (AmSiO$_2$). (d) RLP of typical mineral assemblage of porous interior "mush zone," with blocky pyrite/marcasite, chalcopyrite, and sphalerite (Sp). (e) RLP of a midtemperature to high-temperature mineral assemblage consisting of blocky and dendritic marcasite and minor pyrite, with lesser, later stage chalcopyrite followed by sphalerite. (f) Combined reflected and transmitted light photomicrograph (RLP/TLP) of late-stage bladed barite (Ba) growing off of pyrite in a pore space in the outer layer. Late-stage amorphous silica coats all sulfide phases.

were soaked in fresh water overnight, in order to minimize future salt crystallization and reduce drying time, and subsequently air dried for at least 24 h. Biological material was removed from the solid exterior of the samples. Due to their high porosity, the samples were further dried in a 30°C oven for up to 3 weeks to remove any remaining moisture.

3.2. Spectroscopy and XRD

Midinfrared thermal emissivity spectroscopy, visible/near-infrared (VNIR) reflectance spectroscopy, Mössbauer spectroscopy, and XRD analysis were run on the friable material scraped and dried from each chimney wall. Midinfrared thermal emissivity spectra were acquired using a Nicolet Nexus 670 FTIR interferometric spectrometer at the Arizona State University Mars Space Flight Facility. The spectrometer has been modified for emission measurements by removal of the SiC source and placement of an enclosed glove box and folding mirrors outside the spectrometer housing to enable the energy from a heated sample in a sample chamber within the glove box to enter into the ray path for measurement. The chamber was water cooled to maintain the environmental temperature. The atmosphere was scrubbed of CO$_2$ and H$_2$O to eliminate those spectral lines from the sample data. The spectrometer was equipped with a thermoelectrically stabilized deuterated triglycine sulfate detector and a CsI beamsplitter that allows quality measurement of emitted radiation over the midinfrared range of 2000–240 cm^{-1} (5–42 μm) [e.g., *Ruff et al.*, 1997]. For each measurement, the sample was placed in a copper sample cup, painted with Aeroglaze® Z302 gloss black paint, and heated to and maintained at an 80°C set-point for the duration of the measurements. The 160 scans of each sample were acquired at ∼4 cm^{-1} spectral resolution (∼2 cm^{-1} spectral sampling) and the individual-scan spectra were averaged together. This resulting sample radiance spectrum was calibrated according to the procedure discussed in detail in *Ruff et al.* [1997] and converted to spectral emissivity. No additional spectral filtering was performed.

VNIR reflectance spectra were measured for particulate samples in a horizontal sample dish using a bidirectional VNIR spectrometer and a Nicolet FTIR spectrometer at Brown University's RELAB as in past studies
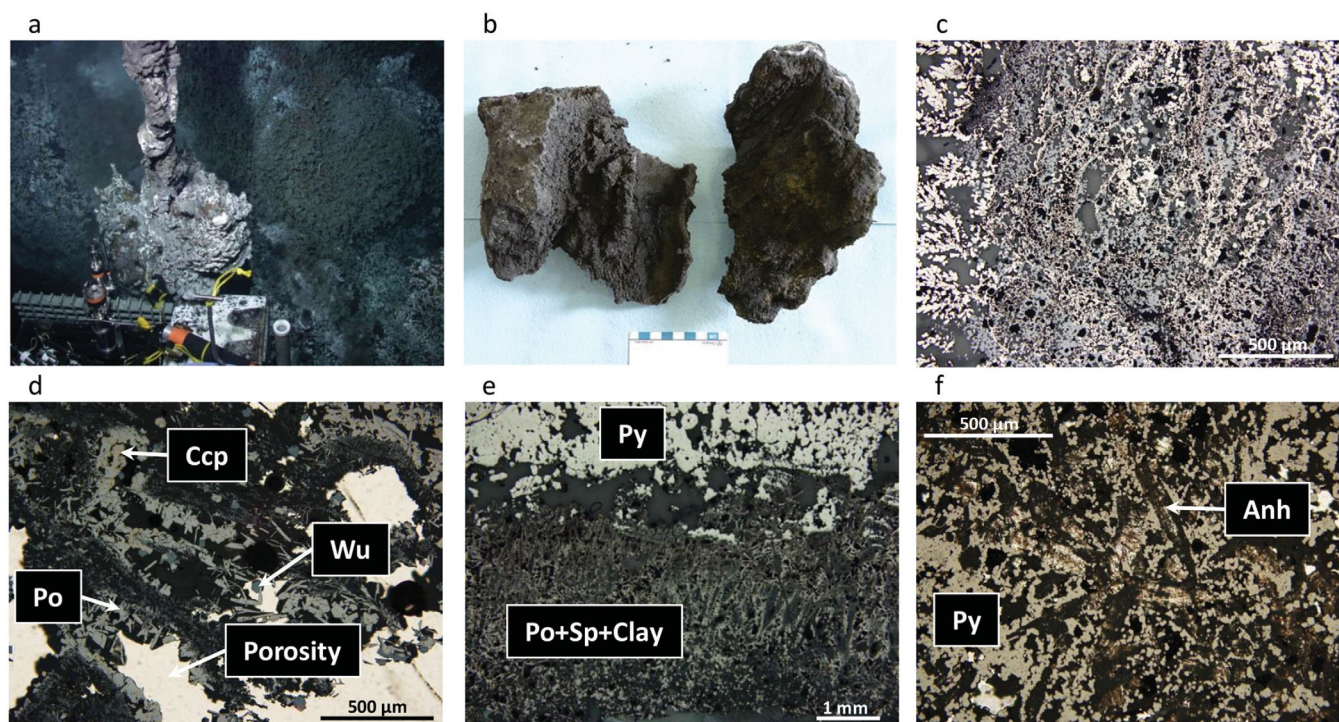
Figure 3. Dante chimney sample. (a) Hydrothermal chimney actively venting 300°C fluid as seen on the seafloor prior to collection. (b) The hydrothermal chimney fragments as seen on board ship prior to subsampling. (c) RLP of typical pyrite-rich and sphalerite-rich mush of the interior wall. (d) RLP/TLP of bladed pyrrhotite (Po), hexagonal wurtzite, minor chalcopyrite (yellow), and fine sphalerite in a dark grey clay matrix. (e) RLP of sharp contact with inner pyrite (top) and outer pyrrhotite with clay minerals and sphalerite. (f) RLP/TLP of semimassive colloform pyrite with interstitial anhydrite (Anh).

[*Bishop et al.*, 2008]. Spectra were measured relative to Halon from 0.3 to 2.5 μm under ambient conditions with 5 nm spectral sampling [e.g., *Pieters*, 1983]. Infrared reflectance spectra were measured relative to a rough gold surface in a biconical configuration with 2 cm^{-1} spectral sampling from 1 to 50 μm in an environment purged of H_2O and CO_2 for 10–12 h. Composite, absolute reflectance spectra were prepared by scaling the FTIR data to the bidirectional data near 1.0 μm.

Mössbauer spectra were acquired at temperatures ranging from 4 to 295 K using a source of ∼40 mCi ^{57}Co in Rh on a WEB Research Co. model WT302 spectrometer equipped with a Janis closed cycle He cooling system at Mount Holyoke College. For each sample, about 80 mg of material were diluted with sucrose and deposited without packing into a holder backed by Kapton® polyimide film tape. Data were collected over a ±4 mm s^{-1} (for spectra containing only doublets) or ±10 mm s^{-1} (for spectra containing sextets) velocity range in 2048 channels with acquisition times ranging from 12 h to 6 d depending on the Fe content of the samples. Spectra were corrected for nonlinearity via interpolation to a linear velocity scale, which is defined by the spectrum of the 25 μm Fe foil used for calibration. All data were corrected to remove the fraction of the baseline due to the Compton scattering of 122 keV gamma rays by electrons inside the detector. All Mössbauer data are available for public use (www.mtholyoke.edu/courses/mdyar/database/).

Mineralogy was also characterized by XRD. XRD sample preparation and analysis were performed by Activation Laboratories Ltd. (www.actlabs.com, Ancaster, Ontario, Canada). Each sample was hand ground in a ceramic mortar using methanol, and a portion of the powder was mounted onto a standard holder. Samples were analyzed on a Panalytical X'Pert Pro diffractometer, equipped with a Cu X-ray source and an X'Celerator detector, operating at the following conditions: 40 kV and 40 mA; range 4.5–80° 2θ; step size 0.017° 2θ; time step 50.165 s; fixed divergence slit, angle 0.25°; sample rotation: 1 rev s^{-1}.

3.3. Petrography and Elemental Analyses

For the Bastille and Dante samples, two thin sections (30 μm thickness) were cut from each whole sample for petrographic analysis. No thin section was cut from the Hot Harold chimney due to the small size of the sample. For the Bastille and Dante chimneys, each section was cut perpendicular to the long axis (and
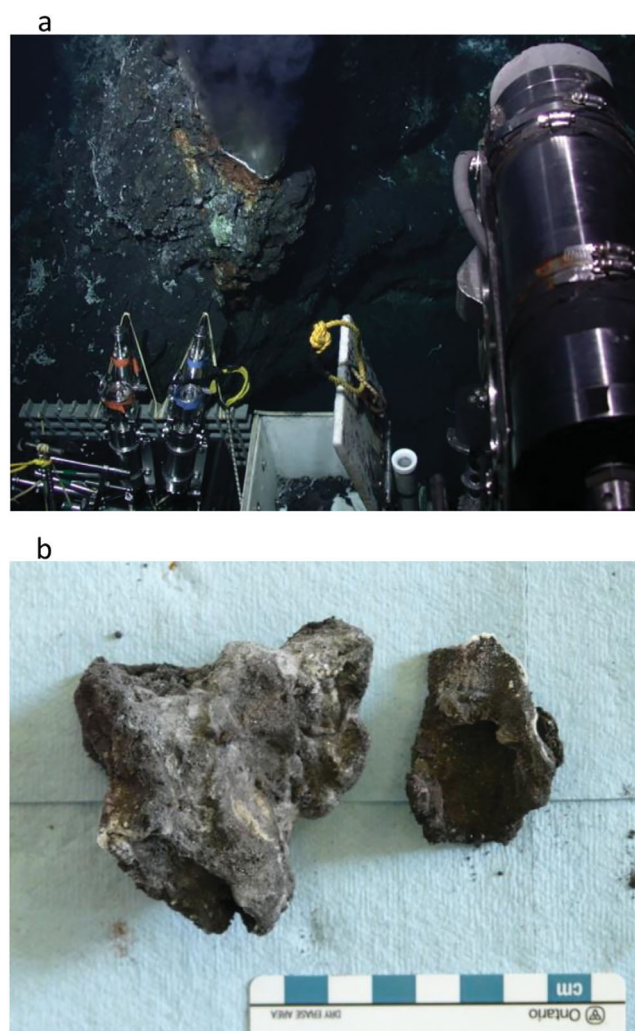
Figure 4. Hot Harold chimney sample. (a) Hydrothermal chimney actively venting 321°C fluid as seen on the seafloor prior to collection. (b) The hydrothermal chimney fragments as seen on board ship prior to subsampling.

primary flow direction) of the chimney to maximize cross-sectional coverage from the outer wall toward the inner conduit zone. Sections were cut such that one section would be representative of the inner zone and the other would be representative of the outer zone. Due to the high porosity and fragility of the chimneys, samples were impregnated with epoxy prior to being cut. Cutting and grinding the friable midwall mineral material was unsuccessful due to its high porosity. The sections were examined using an Olympus BX 51 polarizing microscope with an attached Olympus DP71 digital camera. Both transmitted and reflected light modes were utilized to document the mineralogy.

Representative subsamples of each chimney were broken off and ground to powders (<100 μm) with a tungsten carbide swing mill for major element analysis. For each chimney, three samples were prepared for geochemical analysis: the friable porous midwall of the chimney, material from the outer wall, and a representative whole rock sample. The Hot Harold chimney fragment was too small for an outer wall subsample; therefore, only midwall and whole rock samples were analyzed. Elemental concentrations were determined by a combination of fusion inductively-coupled plasma mass spectrometry and neutron activation analysis at Activation Laboratories Ltd., in Ontario. Analytical uncertainties were determined from repeat analyses of laboratory standard materials.

3.4. Fluid Chemistry

For end-member hydrothermal fluid sampling, duplicate titanium major fluid samplers and gas-tight fluid samplers were used to collect fluids from Bastille. The Hydrothermal Fluid and Particle Sampler (HFPS) was used to collect duplicate fluids from Dante and Hot Harold. The HFPS pumped vent fluid at its maximum stable temperature through a titanium nozzle that measured the temperature of the fluid at 1 Hz just inside the nozzle tip. HFPS fluid sample containers were either PVC piston samplers or titanium piston samplers. All samplers have check valves to prevent the samples from leaking out or being drawn out of the containers. Sample valves were closed upon arrival on deck, and samples were stored under refrigeration until processed. Fluid samples were analyzed on board ship for pH, alkalinity, ΣH_2S, dissolved silica, and ΣNH_3. Subsamples were taken directly from the piston samplers into syringes without exposure to air for shipboard analysis of CH_4 and H_2 by gas chromatography. If a gas headspace was present, then the gas phase and liquid phase volume were measured, and both phases were sampled and analyzed by gas chromatography. Piston samples from the HFPS that were intended primarily for gas analyses were extracted on the same shipboard gas extraction line used for titanium gas-tight samplers, and the gases sealed for later analysis. The extraction water (acidified with sulfamic acid) was analyzed for major elements on shore. Major, minor,

**Table 1.** Inorganic Redox Reactions (From *Amend et al.* [2011])

Aerobic sulfide oxidation	$H_2S + 2O_2 \rightarrow SO_4^{2-} + 2H^+$
Aerobic methane oxidation	$CH_4 + 2O_2 \rightarrow CO_2 + 2H_2O$
Aerobic hydrogen oxidation	$2H_2 + O_2 \rightarrow 2H_2O$
Hydrogenotrophic methanogenesis	$4H_2 + CO_2 \rightarrow CH_4 + 2H_2O$
Hydrogenotrophic sulfate reduction	$4H_2 + SO_4^{2-} + 2H^+ \rightarrow H_2S + 4H_2O$
Anaerobic oxidation of methane	$CH_4 + SO_4^{2-} + 2H^+ \rightarrow CO_2 + H_2S + 2H_2O$

and trace elements in the hydrothermal fluids were analyzed at the Pacific Marine Environmental Laboratory and at the University of Washington. Analytical methods for major and minor elements were described previously [*Butterfield et al.*, 1997; *Edmond et al.*, 1992].

3.5. Redox Energy Estimates

Six redox reactions were considered for microbial energy availability estimates (Table 1). Three of them represent aerobic respiration of inorganic electron donors (sulfide oxidation, methane oxidation, hydrogen oxidation), and three others represent anaerobic respiration of inorganic electron donors (methanogenesis, sulfate reduction, anaerobic oxidation of methane) as previously described [*Amend et al.*, 2011]. All compounds are in the aqueous phase. The compositions of the conservatively mixed hydrothermal solutions were calculated from those of the end-member vent fluids and seawater using the REACT module with its default settings in the computer code Geochemist's Workbench^{TM} as previously described [*Amend et al.*, 2011; *Jin and Bethke*, 2005]. The seawater composition was as previously described [*Amend et al.*, 2011], except O_2 (70 µmol/kg) that was based on O_2 measurements at 2200 m depth within the Endeavour Segment axial valley (R. Thomson, personal communication, 2015).

The reaction path mimics the incremental titration of small aliquots of seawater into hot vent fluid with reevaluation of the chemical speciation of the mixed solution at each step. All minerals were allowed to precipitate and dissolve in the model during mixing except quartz, tridymite, cristobalite, chalcedony, and talc (modified from *Jin and Bethke* [2005]). H_2S, CH_4, H_2, and NH_4^+ were decoupled from redox reactions, but all other redox reactions were allowed. Mineral precipitations at temperatures ranging from 8 to 300°C were predicted from the output of the mixing model. Values of Gibbs energy (ΔG_r) for the catabolic reactions were computed using the activities of relevant species as previously described [*Amend et al.*, 2011]. For example, for the chemical reaction,

$$mA + nB \rightarrow yC + zD$$
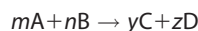
where A and B are the reactants, C and D are the products, and m, n, y, and z are the stoichiometric values, the Gibbs energy is calculated as,

$$\Delta G_r = \Delta G^\circ_T + RT \cdot \ln \left(\frac{\{C\}^y \cdot \{D\}^z}{\{A\}^m \cdot \{B\}^n} \right)_T$$

where ΔG°_T is the standard Gibbs energy at temperature T as provided in *Amend and Shock* [2001], R is the universal gas constant, T is Kelvin temperature, and {} is the activity at temperature T. The amount of energy available (J) from catabolic reactions at mesophilic (25°C), thermophilic (55°C), and hyperthermophilic (80°C) temperatures in a kg of mixed fluid was calculated by multiplying the calculated Gibbs energy for the reaction at each temperature by the concentration of the reactant that was in limiting supply [*Amend et al.*, 2011]. The model was also run separately for comparison as previously described [*McCollom and Shock*, 1997; *Tivey*, 2004] where all mineral precipitations were inhibited and H_2 and O_2 were in equilibrium.

3.6. Microbiology

DNA was extracted from the soft friable midwall material from each chimney that had been frozen on the ship. The extraction was based on a CTAB extraction protocol [*Huber et al.*, 2003]. Approximately 1 g of chimney material was transferred into microfuge tubes and mixed with 0.5 mL of buffer that consisted of 200 mM NaCl, 200 mM Tris-HCl, 2 mM sodium citrate, 10 mM CaCl$_2$, and 50 mM EDTA (pH 8.0). Then 20 µL of 10% sodium pyrophosphate, 30 µL of lysozyme (100 mg/mL), and 20 µL of Poly A (10 mg/mL) were added to the suspension, and the sample was incubated at 37°C for 40 min. Next, 10 µL of 20% sodium dodecylsulfate (SDS) and 60 µL of proteinase K (20 mg/mL) were added and the sample was incubated at 50°C for 30 min. Following this, 80 µL of 5 M NaCl and 80 µL of 10% cetyltrimethyl ammonium bromide (CTAB) in 0.7 M NaCl were added. The sample was mixed well and incubated at 50°C for 30 min. Glass beads (0.1 mm diameter) were added to the tube and the sample was shaken in a Beadbeater shaker for 20 s. The

sample was mixed with 500 μL of phenol:chloroform:isoamyl alcohol (25:24:1) and spun in a centrifuge at 12,000 × g and 4°C for 20 min. The supernatant was then decanted into a clean microfuge tube. The previous step was repeated 1–2 times. Because of low DNA yields, the Dante and Hot Harold samples were transferred to dialysis tubing and suspended in TE buffer (10 mM Tris and 1 mM EDTA, pH 8.0) overnight at 4°C. The DNA was precipitated overnight by adding an equal volume of isopropanol and 0.1 volumes of 3 M sodium acetate. The samples were spun at 12,000 × g at 4°C for 20 min, the pellet was washed with 70% ethanol, and the dry pellet was resuspended in TE buffer.

Polymerase chain reaction was performed to amplify a fragment of the 16S rRNA genes present in these samples with universal bacteria specific primers 27Fb (5′-AGA GTT TGA TCM TGG CTC AG-3′) and 1492Rb (5′-RGY TAC CTT GTT ACG ACT T-3′), and universal archaea specific primers 21Fa (5′-TTC CGG TTG ATC CYG CCG GA-3′) and 958Ra (5′-YCC GGC GTT GAM TCC AAT T-3′). Each PCR contained 7 μL of ddH2O, 2.5 μL of 20% acetamide, 12.5 μL of GoTaq Green mastermix (Promega), 0.25 μL of each 10 μM primer, and 2.5 μL of DNA (undiluted, 1/10 dilution, or 1/100 dilution from the extracted DNA). The DNA was amplified using the following program: 2 min at 94°C, followed by 30 cycles of 94°C for 50 s, 55°C for 45 s, and 72°C for 2 min with a final incubation at 72°C for 10 min. The PCR products were visualized on a 1% agarose gel that had been stained with ethidium bromide. Amplification products were reconditioned to minimize heteroduplexes [*Thompson et al.*, 2002]. Cloning was performed with a TOPO-TA cloning kit (Invitrogen) according to the manufacturer's instructions. Clones were chosen for sequencing by amplification with M13 primers as described previously [*Huber et al.*, 2003] and sequenced with 519Rb (5′-GWA TTA CCG CGG CKG CTG-3′) for bacteria and 515Ra (5′-TTA CCG CGG CKG CTG RCA C-3′) for archaea. All sequences are deposited in GenBank under accession numbers KF578145–KF578374.

For phylogenetic analyses, bacterial and archaeal 16S rRNA gene nucleotide sequences were aligned using ClustalX2 [*Larkin et al.*, 2007] and the Greengenes reference alignment files in Mothur phylogenetic software [*Schloss et al.*, 2009]. Clones were checked for chimeric sequences using both the Bellerophon server [*DeSantis et al.*, 2006] and UChime [*Edgar et al.*, 2011] within Mothur and Qiime [*Caporaso et al.*, 2010]. Operational taxonomic units (OTUs) were then built [*Edgar*, 2010] using a cutoff of 97% to reference sequences; both closed and open reference databases were used and the latter was chosen as the standard in Qiime. Taxonomies were assigned based on the Greengenes taxonomy and a Greengenes reference database [*McDonald et al.*, 2012; *Werner et al.*, 2012] and the RDP Classifier 2.2 [*Wang et al.*, 2007].

Abundances of culturable hyperthermophilic iron reducers, methanogens, and heterotrophic sulfur reducers were estimated using three-tube most-probable-number (MPN) estimates at 85°C as previously described [*Ver Eecke et al.*, 2009, 2012]. The methanogen and heterotroph results were reported previously [*Ver Eecke et al.*, 2012].

4. Results

4.1. Sample Descriptions and Compositions

4.1.1. Bastille

The sample collected from the top of the Bastille edifice was an active black smoker chimney venting 282°C fluid from a central conduit (Figure 2a). It was heavily colonized by *Ridgeia* tubeworms, *Paralvinella* polychaete worms, and scale worms (Figure 2b). The interior was composed of loosely consolidated sulfide material and hosted numerous interior conduits with varying diameters (<5 cm). The conduits were commonly lined with a ~1 mm thick rind of euhedral chalcopyrite (Figure 2b). Some conduits were also lined with a very narrow (<2 mm) secondary rind of sphalerite or marcasite (Figure 2c). The highly porous interior "mush" consisted of a mixture of pyrite, marcasite, chalcopyrite, and sphalerite (Figure 2d).

The exterior walls of the sample consist of a grey matrix of marcasite/pyrite, sphalerite, and amorphous silica, with minor chalcopyrite (Figure 2e). Barite commonly lines the pore spaces within the outer chimney wall, and there is a higher abundance of amorphous silica that commonly coats all exposed mineral surfaces (Figure 2f). The difference in the major element abundances of the inner and outer portions of the sample, reported in Table 2, such as higher Cu concentrations in the interior, and higher Zn and SiO_2 concentrations in the outer portions, reflect the observed mineral distribution in the sample. The porosity of the hand sample, estimated visually, ranges from 10% to 50% in the outer wall and up to 70% in the midwall portions.

Table 2. Major Element Concentrations of Rock Samples, Divided into Analyses of Material From the Inner Fluid Conduits (Used for Microbial Culturing), Outer Chimney Walls and Total Bulk Composition[a]

	Analytical Method[b]	Bastille			Dante			Hot Harold	
		Inner	Outer	Bulk Sample	Inner	Outer	Bulk Sample	Inner	Bulk sample
Fe%	INAA	33.00	33.10	31.50	0.73	38.60	3.86	19.10	0.91
Cu%	ICP-OES	10.00	2.18	4.64	0.11	0.48	1.18	0.33	0.09
Zn%	ICP-OES	2.03	6.31	3.33	0.68	0.44	0.20	0.83	1.29
S%	IR (Leco)	40.2	43.4	40.2	25.7	40.5	27.4	34.1	25.6
SiO_2%	ICP-OES	4.62	6.93	3.29	0.24	0.26	0.19	<0.02	0.90
Ba%	INAA	0.48	0.42	0.40	0.09	0.01	0.03	0.04	0.07
Al_2O_3%	ICP-OES	1.47	0.34	0.45	0.02	0.06	0.02	<0.02	0.02
Pb%	ICP-MS	0.03	0.06	0.04	0.01	0.03	0.00	0.02	0.01
CaO%	ICP-OES	0.10	<0.01	4.88	39.46	7.82	37.22	24.91	38.90
MgO%	ICP-OES	0.05	<0.02	0.02	0.15	0.18	0.07	<0.02	0.5
Na_2O%	ICP-OES	0.53	0.08	0.22	0.67	0.89	0.27	0.47	0.54
Total[c]		92.5	92.8	89.0	67.9	89.3	70.4	79.8	68.8

[a]The results are reported in concentrations of elemental and oxide weight percent (wt %).
[b]INAA, Instrumental Neutron Activation Analysis; ICP-OES, Inductively Coupled Plasma-Optical Emission Spectroscopy; IR, Infrared Detection; ICP-MS, Inductively Coupled Plasma-Mass Spectrometry.
[c]Low totals are largely attributed to the exclusion of sulfate-bonded oxygen in the analyses.

The exterior of the chimney is coated in 5 mm of marcasite crust with minor white bacterial and minor red oxidized coatings.

4.1.2. Dante

The sample collected from the top of the Dante edifice was the bulbous base of a beehive-like chimney that was diffusely venting clear fluid at 300°C (Figure 3a). The midwall portion is black/brown (Figure 3b) and highly porous, and is composed primarily of pyrite and sphalerite (Figure 3c). Although anhydrite was not observed in this particular thin section, the high Ca content in the interior of the samples indicates a high abundance of anhydrite in the midwall portion as well (Table 2). Flow channels, 0.5–2 cm in diameter, are lined by euhedral chalcopyrite, pyrrhotite, and wurtzite (Figure 3d). Dark brown to black bladed pyrrhotite crystals (up to 3 mm long) within the porous interior of the chimney are uniformly aligned with an along-axis orientation. There is a clear concentric zonation of pyrite and pyrrhotite-wurzite-rich areas away from the central fluid conduit (Figure 3e).

A 7 mm wide crust forms the outermost layer, and is composed primarily of pyrite, marcasite, and lesser anhydrite (Figure 3f and Table 2). Amorphous silica that encases sulfide minerals increases in abundance toward the exterior and likely represents late-stage precipitation [*Hannington et al*., 1995; *Tivey et al*., 1999]. The chimney exterior is gray with white bacterial mat and Fe-staining and hosted few *Paralvinella* polychaete worms.

4.1.3. Hot Harold

The Hot Harold sample was collected from the northern-most end of the Faulty Towers complex (Figure 4). This parasitic chimney has been routinely sampled since its discovery in 1996 [*Kelley et al*., 2001] and hence, the sample is young. The candelabra-like regrowth was vigorously venting 321°C black smoker fluid from a >10 cm orifice at the base of the chimney (Figure 4a). The sample is marked by several narrow (<14 mm diameter) conduits (Figure 4b). The mineralogy is dominated by fine-grained, dark gray/black pyrite, and sphalerite and bladed (<2 mm long) euhedral anhydrite. White/buff coloration of the exterior walls likely resulted from bacterial mat growth. Chalcopyrite is more abundant in the interior, and sphalerite is more abundant toward the exterior. The relatively high Ca indicates the presence of high amounts of anhydrite in the sample (Table 2).

4.2. XRD and Mineral Spectroscopy

XRD and mineral spectroscopy were performed on the air dried material scraped from the friable midwall portion of the chimney. A comparison of the mineral identifications using various techniques is provided in Table 3. XRD analysis indicates that the Bastille sample contains pyrite, chalcopyrite, and marcasite, as well as gypsum in one of the two replicates. It confirms optical mineral identifications, but also indicates the presence of seawater-derived minerals such as gypsum. Analysis of the Dante sample shows it contains anhydrite, pyrite, minor gypsum, lepidocrocite, and native sulfur and largely confirms optical mineral identifications. XRD analysis of the Hot Harold sample shows it contains only anhydrite and minor gypsum.

Table 3. Comparison of Analytical Results for Mineralogy

Technique	Scale	Bastille	Dante	Hot Harold
Petrography	Microscale, all	Marcasite,[a] pyrite,[a] chalcopyrite,[a] sphalerite,[a] silica,[b] barite,[b] and anhydrite[b]	Anhydrite,[a] pyrite,[a] pyrrhotite,[a] sphalerite,[a] wurtzite,[a] and iron oxide[b]	Not available due to small sample size
Elemental analysis	Bulk, all	Relatively abundant Fe, Ba, and SiO_2; Cu and Al_2O_3 high in inner wall; Zn high in outer wall	CaO high in inner wall, Fe high in outer wall	Relatively abundant CaO
X-ray diffraction	Bulk, interior	Pyrite,[a] marcasite,[a] chalcopyrite,[a] and gypsum[b]	Anhydrite,[a] pyrite,[a] gypsum,[b] and sulfur[b]	Anhydrite,[a] and gypsum[b]
VNIR reflectance spectroscopy	Bulk, interior	Chalcopyrite and/or pyrite,[a] mica,[b] and chlorophyll-a[b]	Anhydrite,[a] chalcopyrite and/or pyrite,[a] gypsum,[b] and chlorophyll-a[b]	Anhydrite,[a] gypsum,[b] sphalerite, and/or pyrite[b], possibly sulfur[b]
Thermal emission spectroscopy	Bulk, interior	Chalcopyrite and/or pyrite[a]	Gypsum,[a] and pyrite[b]	Anhydrite[a]
Mössbauer spectroscopy	Bulk, interior	Chalcopyrite (sextet),[a] possible pyrite, sphalerite, marcasite (doublet)	Possible pyrite, sphalerite, marcasite (doublet), possible ferricopiapite, lepidocrocite, maybe schwertmannite (sextets)	Too little Fe to identify minerals

[a]Major component.
[b]Minor component.

Visible/near-infrared (VNIR) reflectance spectra of all three samples were very dark, consistent with the presence of pyrite, chalcopyrite, and sphalerite that were identified using other techniques (Figure 5). Two broad bands observed near 1 and 2 μm in spectra of the Bastille samples are characteristic of Fe^{2+} excitations in pyrite (Figure 5a). The wavelength positions of these bands are highly dependent on mineral chemistry [*Burns*, 1993], and the band centers near 0.90 and 1.80 μm could be due to pyrite with a composition different from that available in spectral libraries. The sharp bands at 2.73–2.75 μm are due to OH stretching vibrations and are characteristic of phyllosilicates. A broadening of the 0.9 μm Fe^{2+} band toward 0.85 μm for both Bastille samples is attributed to a Fe^{3+} electronic transition, as found in iron oxide minerals such as hematite or Fe^{3+} in some clays and sulfate phases. Based on the areas of the peaks in this region, it is estimated that a small amount of mica containing some Fe^{3+} such as zinnwaldite was present in this sample. The sharp band at 0.662 μm is indicative of chlorophyll *a*, while the additional sharp band at 0.87 μm is indicative of bacteriochlorophyll *a* [e.g., *Hubas et al.*, 2011; *Pierson et al.*, 1987]. Another sharp weak band near 0.975 μm may also be due to a pigment from an anaerobic microorganism as it is narrower than typically observed for Fe transitions.

The dominant features in the VNIR spectra of the Dante and Hot Harold samples (Figure 5b) were H_2O and SO_4 bands characteristic of Ca sulfates [*Bishop et al.*, 2014]. The Hot Harold spectrum exhibited a suite of sharp bands from 4.2 to 5 μm that indicate anhydrite. The broader bands near 4.5 and 4.7 μm in the spectrum of Dante are consistent with a mixture of anhydrite and gypsum. A H_2O stretch plus bend combination band near 1.94 μm in the spectra of both Dante and Hot Harold samples indicates that both samples contained H_2O in the mineral structure [note that the anhydrite laboratory spectrum also contains this band but that is not due to anhydrite, *Bishop et al.*, 2014]. Due to the presence of this H_2O band, Hot Harold likely contained some gypsum as well as anhydrite, although anhydrite is spectrally dominant. The Dante spectrum also contained a weak chlorophyll band at 0.662 μm. A rather unusual reflectance maximum was observed near 0.58 μm for Bastille and Dante. It could be caused by a mixture of chalcopyrite and pyrite or it could also be consistent with the sulfate coquimbite, which has a maximum at 0.47 μm and is produced by oxidation of those sulfides. Although coquimbite has not been identified with other techniques, its structure is similar to that of many other sulfates, so its presence could easily be overlooked if it is mixed with other sulfates and sulfides. The increasing spectral slope observed for Hot Harold samples was attributed to a mixture of a Fe^{2+} phase with the other minerals. The difference in spectral shape from 0.5 to 1.8 μm in the Hot Harold spectrum compared to spectra of the other samples in the study could be explained by the presence of sphalerite instead of chalcopyrite as the darkening agent. The spectrum of sulfur also exhibits a
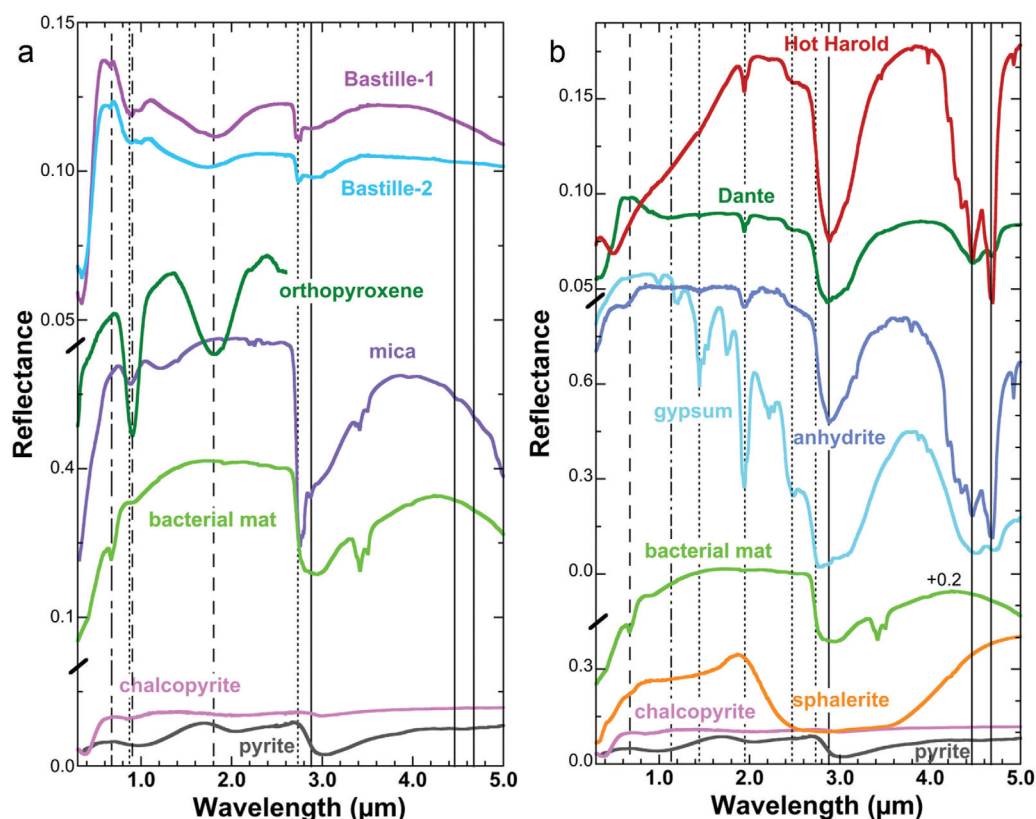
Figure 5. Reflectance spectra are shown from 0.35 to 5 μm for the Bastille, Dante, and Hot Harold samples together with spectra of likely minerals present in the samples. (a) VNIR spectra of Bastille-1, Bastille-2, orthopyroxene DL064 [*Klima et al.*, 2007], zinnwaldite mica JB729 [*Bishop et al.*, 2008], JB205, a chlorophyll-bearing bacterial mat from beneath Lake Hoare in the Antarctic Dry Valleys [*Bishop et al.*, 2001], chalcopyrite HS431 [*Clark et al.*, 2007], and pyrite GDS483 [*Clark et al.*, 2007]. (b) VNIR spectra of Hot Harold, Dante, anhydrite GDS42 [*Clark et al.*, 2007], gypsum JB567 [*Bishop et al.*, 2014], chlorophyll-bearing mat JB205, sphalerite HS136 [*Clark et al.*, 2007], chalcopyrite HS431, and pyrite GDS483.

minimum near 0.4 μm [*Clark et al.*, 2007], but is spectrally too bright in the NIR to be a major component of this sample.

The thermal emission spectra (Figure 6) are fairly simple because each spectrum was dominated by a single identifiable mineral. Complex mixtures of minerals were not present. Laboratory spectra of pure mineral sulfide and sulfate phases [*Lane*, 2007, 2008] are shown in Figure 6 for comparison to the Endeavour chimney samples. Both Bastille sample spectra clearly indicate iron sulfide (chalcopyrite and/or pyrite), but no sulfate. Gypsum was found in Dante, with possible trace pyrite. Anhydrite is clearly identified in Hot Harold.

Mössbauer data for the chimney samples and several sulfide and sulfate standards are shown (Figure 7 and supporting information Table S1), with spectra normalized to 1% absorption. The Mössbauer data were very consistent with the Fe-rich sulfide phases identified by thermal emission spectroscopy. Room-temperature spectra of Bastille contain a central doublet and sextet consistent with that in the chalcopyrite standard. The relative increase in the area of the central doublet in Bastille as compared to chalcopyrite is likely due to contribution from pyrite, marcasite, or sphalerite. This doublet broadens, but does not split at 4 K, ruling out ferricopiapite, fibroferrite, schwertmannite, lepidocrocite, and hematite as possible constituents. Dante spectra are also dominated by a doublet that persists to 4 K, again consistent with pyrite, marcasite, or sphalerite. Several sextet distributions are observed in Dante at 4 K. They are poorly defined, but overlap with sextet distributions of ferricopiapite, lepidocrocite, and possibly schwertmannite. Hot Harold contains little iron (<0.5% absorption with an undiluted sample) and any iron-bearing minerals present could not be identified by Mössbauer spectroscopy.

4.3. Fluid Chemistry

Most of the calculated end-member chemical concentrations for the hydrothermal fluids emanating from Bastille, Dante, and Hot Harold (Table 4) fall within the range of previously measured values for the MEF and
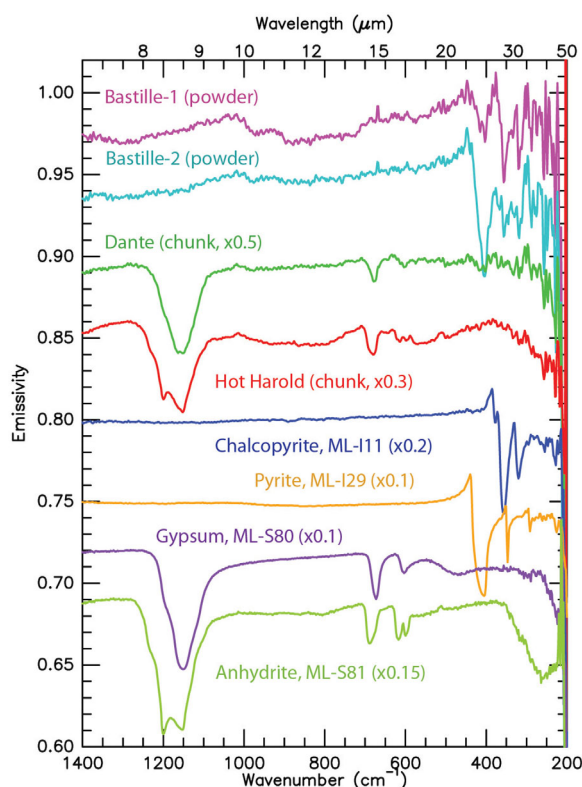
Figure 6. Thermal emissivity spectra of the Endeavour hydrothermal chimney samples and four laboratory mineral spectra for comparison (sulfide spectra are from *Lane* [2008]; sulfate spectra are from *Lane* [2007]). Spectra are offset for clarity.

Mothra fields [*Butterfield et al.*, 1994; *Lilley et al.*, 1993, 2003; *Seewald et al.*, 2003]. Fe^{2+} concentrations, and to a lesser extent Zn^{2+} concentrations, were significantly higher in end-member hydrothermal fluids from Bastille, and were lowest in fluids from Hot Harold. In contrast, Li, Rb, Sr^{2+}, Mn^{2+}, and Cs concentrations were highest in Hot Harold fluids and lowest in Bastille fluids. Otherwise, the chemistries of the three fluids generally were very similar to one another. The pHs of the fluids were mildly acidic at 25°C with ranges of pH 4.0–4.5. H_2 concentrations were slightly low to normal relative to historical values for Endeavour. CH_4 and ΣNH_3 concentrations were typical for Endeavour, but highly elevated relative to global mid-ocean ridge hydrothermal systems. Concentrations of $\Sigma H_2 S$ and SiO_2 were within the range of previously measured values for Endeavour. The Cl^- concentrations of Bastille and Dante were below that of seawater. These values likely reflect that the subsurface fluids have lost a small proportion of condensed brine, while the Cl^- concentration

of Hot Harold in the Mothra field was above that of seawater, reflecting minor brine enrichment [*Butterfield et al.*, 1993, 1997; *Von Damm et al.*, 1995].

4.4. Reaction Energetics

Reaction energetics for the six microbial catabolic processes were evaluated for Bastille, Dante, and Hot Harold and plotted for seawater:hydrothermal fluid mixtures representing a kg of mixed fluid at 25°C, 55°C, and 80°C, or microbial activity at mesophilic, thermophilic, and hyperthermophilic temperatures, respectively (Figure 8). The calculated pH for each fluid is >pH 5 at each of these three temperatures. The predicted temperatures for the transition from oxidized to anoxic conditions are 101°C for Bastille, 117°C for Dante, and 202°C for Hot Harold. For each fluid, 11–35 mg of hematite is predicted to precipitate permanently from the fluid. Anhydrite (2.3–2.6 g) is predicted to precipitate from each fluid but then redissolves back into the fluid as the titration of seawater into hydrothermal fluid continues and temperature decreases. Similarly, pyrite (29–43 mg) and amorphous silica (20–64 mg) precipitate from Bastille and Dante fluids, but then redissolve back into the mixed fluid as the seawater titration continues. There was no predicted precipitation of pyrite or amorphous silica from Hot Harold fluids. The reaction of O_2 with Fe^{2+} had the most significant impact on the availability of O_2. When mineral precipitation was inhibited and H_2 and O_2 were in equilibrium, the transition temperatures from oxidized to anoxic conditions were 255°C for Bastille and 180°C for Dante and Hot Harold with no H_2 available below these temperatures.

The six reaction energetics representing autotrophic metabolisms do not vary significantly between sites at 25°C, but do vary in magnitude with increasing temperature. At 25°C, aerobic S^{2-} oxidation and CH_4 oxidation provide the largest amount of redox energy for microbial catabolism (18.65–21.54 J/kg and 21.65–24.98 J/kg, respectively). They are both limited by the availability of O_2 in seawater, and thus the energy available for these reactions decreases with increasing temperature. The effect is greatest in Bastille (4.69 J/kg and 5.59 J/kg, respectively, at 80°C) followed by Dante (7.50 J/kg and 8.89 J/kg, respectively, at 80°C)
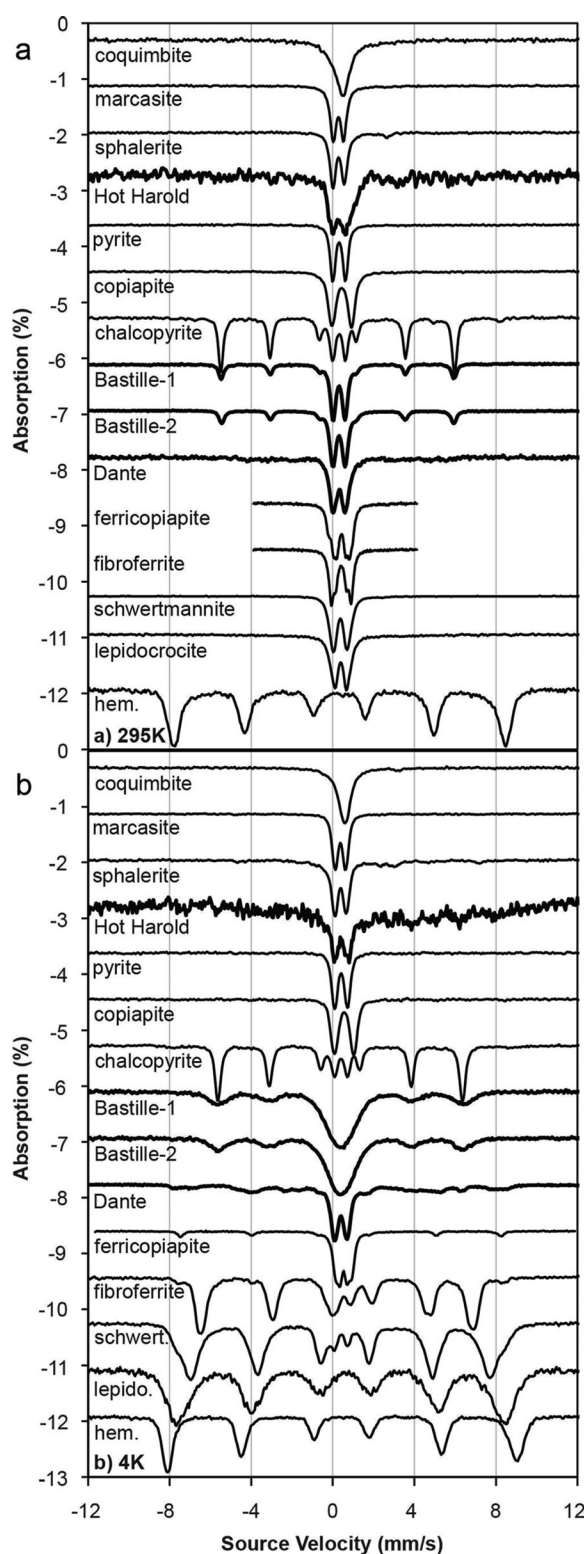
Figure 7. (top) Mössbauer data acquired at 295 K and (bottom) 4 K. Hydrothermal samples are shown with similar minerals. The spectra of Bastille consist of a chalcopyrite sextet and a doublet that could be pyrite, sphalerite, or marcasite. The Dante spectra contain a doublet that could represent pyrite, sphalerite, or marcasite and a sextet that could be ferricopiapite, lepidocrocite, or schwertmannite. The Hot Harold sample had too little Fe to produce an interpretable Mössbauer spectrum.

due to their lower predicted O_2 concentrations at 55°C and 80°C relative to Hot Harold (14.21 J/kg and 16.86 J/kg, respectively, at 80°C). Reaction energies for aerobic H_2 oxidation (0.49–5.04 J/kg), hydrogenotrophic SO_4^{2-} reduction (0.03–0.24 J/kg), methanogenesis (0.04–0.39 J/kg), and anaerobic methane oxidation (0.03–0.10 J/kg) increase with temperature due to the increased availability of H_2, but were substantially lower than the energy available at 80°C for the other two reactions. Other than the reaction of O_2 with Fe^{2+}, the mineral precipitations had no effect on the reaction energy available.

4.5. Microbiology

To compare microbial community compositions, bacterial 16S rRNA gene clone libraries were constructed and resulted in 68, 74, and 62 clone sequences for chimneys from the Bastille, Dante, and Hot Harold edifices, respectively (supporting information Table S2). All of the bacterial clone libraries were largely dominated by *Proteobacteria* (Figure 9), but distributions within subclasses of this phylum varied widely. *Deltaproteobacteria* were found almost exclusively in the Bastille chimney and represented 48% of the total OTUs in that sample. Of these, 45% were most closely related (87–91% identity) to *Desulfobulbus mediterraneus* and 24% were most closely related (84–91% identity) to *Desulfobacterium indolicum* and *Desulfobacterium aniline*. These are mesophilic, obligately anaerobic sulfate reducers [*Bak and Widdel*, 1986; *Sass et al.*, 2002; *Schnell et al.*, 1989]. Another 15% of the *Deltaproteobacteria* sequences were most closely related (82–91% identity) to other mesophilic, obligately anaerobic sulfate reducers, and 9% were most closely related (80–86% identity) to the thermophilic, anaerobic iron reducer *Geothermobacter ehrlichii* [*Kashefi et al.*, 2003]. *Alphaproteobacteria*, *Gammaproteobacteria*, and *Epsilonproteobacteria* were also present at low abundances, along with representatives of the *Bacteroidetes*, *Chloroflexi*, *Deinococcus-Thermus*,

Table 4. Chemical Composition of End-Member Hydrothermal Vent Fluids Extrapolated to Zero-Mg^{2+} (±Standard Error) From This Study and Seawater for Modeling Purposes

	Bastille	Dante	Hot Harold	Seawater[a]
Temperature, max	282°C	300°C	321°C	2°C
pH at 25°C	4.00 ± 0.05	4.25 ± 0.05	4.51 ± 0.05	7.8
SiO_2 (mmol/kg)	16.97 ± 0.20	17.13 ± 0.20	16.10 ± 0.01	0.13
ΣH_2S (mmol/kg)	3.34 ± 0.26	4.00 ± 0.30	4.30 ± 0.11	0
H_2 (μmol/kg)	28.8	87.6	90.0	0
CH_4 (mmol/kg)	1.88	1.55	1.50	0
ΣCO_2 (mmol/kg)	10.8	13.1	7.0	2.2
O_2 (μmol/kg)	0	0	0	70
ΣNH_3 (μmol/kg)	498.2 ± 6.1	452.8 ± 18.3	426.0 ± 2.0	0
Cl^- (mmol/kg)	440.3 ± 9.7	507.8 ± 2.3	655.1 ± 0.7	550
SO_4^{2-} (mmol/kg)	0	0	0	27.9
Na^+ (mmol/kg)	358.4 ± 8.1	399.6 ± 3.4	501.3 ± 0.2	441
Mg^{2+} (mmol/kg)	0	0	0	54.5
K^+ (mmol/kg)	21.2 ± 0.2	27.5 ± 0.8	39.0 ± 0.0	9.8
Ca^{2+} (mmol/kg)	27.7 ± 0.7	38.2 ± 1.2	51.6 ± 0.2	10.7
Fe^{2+} (μmol/kg)	562.6 ± 27.1	442.7 ± 69.3	139.9 ± 1.5	
PO_4^{3-} (μmol/kg)	0.64 ± 0.25	0.53 ± 0.47	0.90 ± 0.05	
Li (μmol/kg)	253.1 ± 27.3	368.1 ± 35.4	516.4 ± 4.1	
Rb (μmol/kg)	20.1 ± 0.7	27.6 ± 1.1	42.6 ± 0.5	
Sr^{2+} (μmol/kg)	101.7 ± 1.6	141.8 ± 24.0	198.0 ± 1.4	
Ba^{2+} (μmol/kg)		1.4 ± 0.4	5.6 ± 0.2	
B (μmol/kg)	608.2 ± 47.8	646.4 ± 37.4	591.5 ± 15.1	
Al^{3+} (μmol/kg)	7.2 ± 1.3	6.1 ± 1.5	6.1 ± 0.5	
Mn^{2+} (μmol/kg)	163.7 ± 3.3	189.3 ± 21.9	292.9 ± 3.5	
Cu^+ (μmol/kg)	11.3 ± 4.0	13.8 ± 0.4		
Zn^{2+} (μmol/kg)	27.7 ± 3.6	17.5 ± 8.2	11.7 ± 6.4	
Cs (nmol/kg)	246.8 ± 6.7	349.4 ± 27.4	532.5 ± 5.6	
Pb (nmol/kg)	112.6 ± 19.1	127.3 ± 97.4		

[a]Seawater composition from *Amend et al.* [2011], except the O_2 concentration which is from Richard Thomson (Institute of Ocean Sciences, Fisheries and Oceans Canada, personal communication, 2015).

Firmicutes, and *Planctomycetes*. The majority of the sequences in the Bastille chimney (74%) were most closely related to mesophilic and thermophilic anaerobes and microaerophiles. A minority of the sequences (20%) were most closely related to obligate and facultative autotrophs.
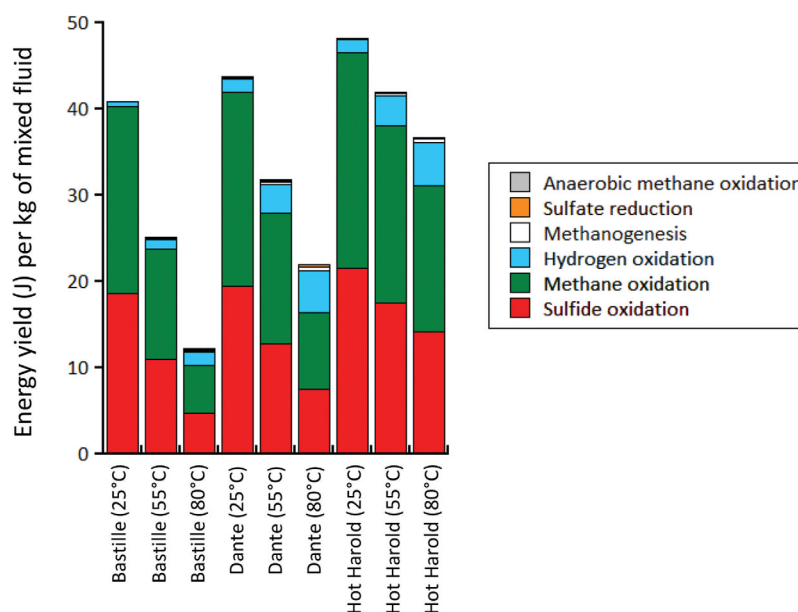

Figure 8. Predicted catabolic energies (in J per kg of mixed fluid) available for anaerobic oxidation of methane (gray), hydrogenotrophic sulfate reduction (orange), hydrogenotrophic methanogenesis (white), aerobic hydrogen oxidation (blue), aerobic methane oxidation (green), and aerobic sulfide oxidation (red) at 25, 55, and 80°C in mixed abiotic hydrothermal-seawater solutions flowing from Bastille, Dante and Hot Harold.
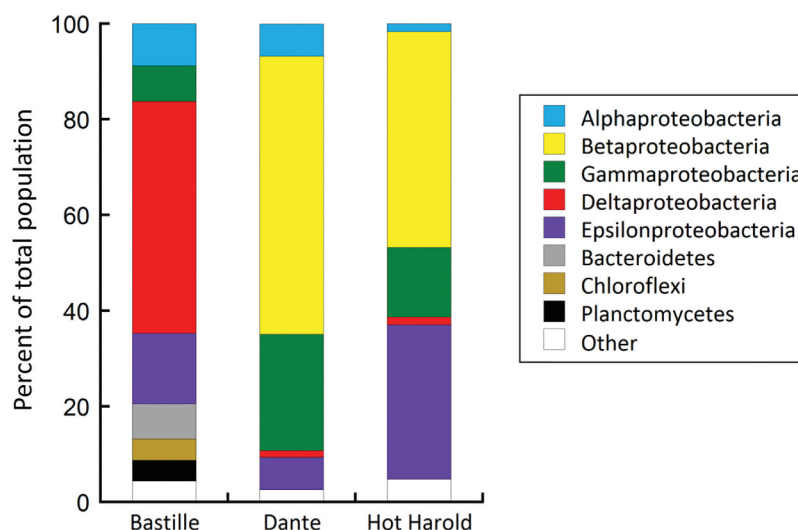
Figure 9. Relative abundances of bacterial taxa observed in Bastille, Dante, and Hot Harold hydrothermal vent deposits.

Within the Dante and Hot Harold chimneys, *Betaproteobacteria* dominated with contributions of 58% and 45%, respectively (Figure 9). Sequences most closely related to *Roseateles depolymerans* comprised 44% and 89% of the *Betaproteobacteria* in Dante (90–99% identity) and Hot Harold (97–98% identity), respectively. Also, 23% of the *Betaproteobacteria* in Dante were most closely related (99% identity) to *Delftia acidovorans*, 12% were most closely related (99–100% identity) to *Ralstonia pickettii*, and 5% were most closely related (99% identity) to *Cupriavidus metallidurans*. These latter three *Betaproteobacteria* are mesophilic aerobes that are highly resistant to heavy metals [*Goris et al.*, 2001; *Wen et al.*, 1999; *Yabuuchi et al.*, 1995]. *Epsilonproteobacteria* comprised 32% of the bacterial sequences in Hot Harold, 15% in Bastille, and 7% in Dante. Sequences most closely related (88–95% identity) to *Sulfurimonas autotrophica* and *Sulfurimonas paralvinella* comprised 60% of the *Epsilonproteobacteria* in Hot Harold. These are mesophilic, autotrophic sulfur-oxidizing aerobes [*Inagaki et al.*, 2003; *Takai et al.*, 2006]. *Alpha-*, *Gammaproteobacteria*, and *Deltaproteobacteria* were also present at much lower percentages along with representatives of *Actinobacteria* and *Cyanobacteria* in Dante and *Aquificae* and *Firmicutes* in Hot Harold. The majority of the sequences from Dante and Hot Harold were most closely related to mesophilic and thermophilic aerobes, but a minority of sequences (14% and 44%, respectively) were most closely related to obligate and facultative autotrophs.

Chao1, Shannon index, and Observed Species diversity indices were calculated in Qiime for bacterial clone libraries from all three samples (supporting information Table S3). These indicated that both Bastille and Dante had relatively higher diversity than Hot Harold in all three diversity indices calculated. However, rarefaction curves indicate that complete saturation of the environment was not reached and therefore no trends in alpha-diversity could be identified. Across samples, the relative distances measured between communities (beta-diversity) using Unweighted UniFrac and Weighted UniFrac [*Lozupone and Knight*, 2005] indicated that Dante and Hot Harold were more similar taxonomically than either of these were with Bastille (supporting information Table S3). In concert, the community structures in the Dante and Hot Harold chimneys are more similar to each other than to those in the Bastille chimney.

Twenty-three archaeal 16S rRNA gene clone sequences were obtained from the Bastille chimney and were primarily related to hyperthermophilic anaerobes (supporting information Table S2). Despite repeated attempts, no archaeal clones could be recovered from either the Dante or Hot Harold chimneys, most likely due to the generally low DNA yield from these samples. *Thermococci* contributed 48% of the total archaeal clones in the Bastille chimney with additional contributions from *Thermoprotei* (17%), *Methanococci* (13%), *Archaeoglobi* (9%), and *Korarchaeota* (9%). The *Thermococci* were most closely related (86–87% identity) to *Thermococcus* spp. (supporting information Table S2), which are hyperthermophilic, heterotrophic sulfur reducers and H_2 producers [*Itoh*, 2003]. The *Thermoprotei* were most closely related to *Hyperthermus butylicus* (92%) and *Vulcanisaeta distributa* (78–93%), which are hyperthermophilic sulfur and iron reducers [*Itoh*

et al., 2002; *Zillig et al.*, 1990]. The *Methanococci* were most closely related (88%) to *Methanocaldococcus* spp., which are hyperthermophilic methanogens [*Whitman and Jeanthon*, 2006]. The *Archaeoglobi* spp. were most closely related to *Ferroglobus placidus* (80%) and *Geoglobus acetivorans* (79%), which are hyperthermophilic iron reducers [*Hafenbradl et al.*, 1996; *Slobodkina et al.*, 2009]. One sequence was most closely related to *Aciduliprofundum boonei* (86%), which is a thermoacidophile that reduces sulfur and iron [*Reysenbach et al.*, 2006]. For both the Bacteria and the Archaea, the use of clone libraries in 2008 limited the number of sequences obtained and the biodiversity measured compared to next-generation Illumina sequencing that is more commonly used today, but does provide longer sequence reads and better sequence annotation than Illumina sequencing.

In general, the interior sulfide sample from the Bastille chimney contained higher numbers of culturable hyperthermophiles than the interior mineral samples from the Dante and Hot Harold chimneys based on MPN estimates (supporting information Table S4). Heterotrophic sulfur reducers were at least ten-fold more abundant in the samples than either iron reducers or methanogens, mirroring the pattern observed with the archaeal clone library from the Bastille chimney.

5. Discussion

5.1. Comparison of Mineralogical Data

The presence of chalcopyrite lining the major fluid conduits within the Bastille sample suggests very little reduction in hydrothermal fluid temperature due to seawater mixing or conductive cooling prior to venting when this mineral formed [*Hannington et al.*, 1995]. Pyrite, marcasite, and sphalerite, which were found in the midwall sulfide zone, typically precipitate at lower temperatures than chalcopyrite in hydrothermal vents, and the presence of these minerals suggests a decrease in vent fluid temperature within this zone as a result of mixing with local seawater and/or conductive cooling through the chimney walls [*Hannington et al.*, 1995]. The overgrowth and recrystallization relationships of high-temperature and lower-temperature sulfide minerals in the midwall portion (Figure 2e) indicate a complex growth history controlled by variations in fluid chemistry, flux, flow patterns and/or mixing during chimney growth. Sphalerite overgrowth of other sulfide phases indicates that it was the latest sulfide phase to precipitate in the outer wall. The temperature-dependent sulfide mineral distribution within the Bastille sample, with a high-temperature chalcopyrite-rich core and lower temperature sphalerite-rich exterior, is also reflected in the bulk geochemical analyses, with relatively high Cu concentrations in the interior and high Zn concentrations toward the exterior of the sample (Table 2). Low Ba and Ca concentrations in both the inner and outer zones indicate limited precipitation of sulfate minerals within the chimney, relative to sulfide minerals and amorphous silica. However, elevated Al_2O_3 concentrations (1.47% in the inner zone, Table 2) likely reflect clay mineral precipitation within the chimney.

For the Dante and Hot Harold samples, the high Ca concentrations indicate that the samples are composed primarily of anhydrite, which precipitated during ingress and heating of seawater through the porous chimney walls (Table 2). Both samples, however, also exhibit typical temperature-controlled sulfide zonation, with high-temperature sulfide minerals (chalcopyrite, wurtzite, and pyrrhotite) in the interior and lower temperature sulfide minerals (pyrite and sphalerite) toward the exterior (Figure 3).

There are two models that can explain the paragenesis of the three sampled chimneys and, in part, the niche partitioning of the types of microbes observed within them. *Goldfarb et al.* [1983] and *Haymon* [1983] describe the growth of hydrothermal chimneys as first forming a highly permeable wall composed of anhydrite and minor sulfides (Stage 1). Over time, the mixing of seawater and hydrothermal fluid through this wall causes the precipitation of additional sulfides and sulfates, which reduces the permeability of the chimney wall. The exterior of the chimneys becomes isolated from the interior flow channel, the interior temperature increases leading to the precipitation of chalcopyrite and other metal sulfide minerals, and the cooler exterior produces minerals by reactions of seawater and the mineral assemblages of the chimney walls (Stage 2). Using this model, the chimneys from the Dante edifice and especially from the Hot Harold edifice are relatively younger chimneys in an earlier stage of development (Stage 1), while the chimney from the Bastille edifice is more mature (Stage 2).

The second model of *Koski et al.* [1994] suggests that the Bastille chimney had focused, rapid fluid flow leading to the formation of a columnar cylindrical chimney with concentric mineral assemblages composed of abundant chalcopyrite, sphalerite and anhydrite (i.e., Type I). In contrast, the fluid flow through the Dante

and Hot Harold chimneys was slower and more diffuse than Type I chimneys leading to a porous anhydrite-rich interior and, in the case of the Dante sample, a pyrite-rich and marcasite-rich exterior shell (i.e., Type II). The extensive macrofauna colonization on the exterior of the Bastille chimney, the chalcopyrite precipitation, and the concentric deposition of mineral assemblages around a central flow channel support the idea that it was more mature than the other two chimneys with focused, rapid fluid flow. The Dante chimney was more mature than the Hot Harold chimney, but both likely had slower and more diffuse fluid flow through them resulting in more mixing with seawater and deposition of more anhydrite. Furthermore, because of the lower Fe^{2+} concentration in its hydrothermal fluid, there was no prediction of the precipitation of pyrite within the Hot Harold sample in the Geochemist's Workbench mixing model (although a very minor amount of pyrite and sphalerite was detected by VNIR) suggesting that it was already limited in its ability to form metal sulfide minerals. Each of these paragenesis models for each chimney helps to explain the differences observed in the microbial communities in the Bastille chimney relative to the other two chimneys, namely the maturity of the chimney, the fluid chemistry flowing through it, and the physical nature of the fluid flow. While conservative mixing models generally predicted the minerals precipitated in the chimneys accurately, they were unable to take into account physical fluid flow characteristics and maturity of the structure and how those affect the condition within the chimneys.

Our study used for the first time Mössbauer spectroscopy and reflectance and emission spectroscopic techniques (VNIR and thermal emissivity) to analyze the minerals in actively venting deep-sea hydrothermal chimneys. In this study, midinfrared emission analyses rapidly and accurately identified the major mineral components in samples from all three chimneys (chalcopyrite, pyrite, anhydrite) in agreement with the major phases detected by XRD. Using VNIR reflectance spectra, anhydrite and gypsum also were readily identified in the Dante and Hot Harold samples. However, because the shorter-wavelength spectra of all samples were very dark (i.e., low reflectivity), consistent with the presence of sulfides such as chalcopyrite, pyrite, sphalerite, these phases could not be uniquely identified. Minor amounts of mica were detected in the VNIR spectra of the Bastille samples that were not detected by XRD or midinfrared spectra. However, VNIR spectra are generally more sensitive to the presence of mica than other techniques (although midinfrared emissivity data are also sensitive to clay minerals if coarser or more abundant).

Reflectance and emission spectroscopy techniques also detected biological signals. The VNIR spectral analyses indicated the presence of chlorophyll *a* in the Bastille and Dante samples and bacteriochlorophyll *a* in the Bastille samples. While the presence of chlorophyll is seemingly inconsistent with the deep-sea endolithic source of the samples, the Bastille 16S rRNA gene clone library contained two *Chlorobaculum*-like sequences (anaerobic, green sulfur photosynthetic bacteria) and a *Thalassobacter stenotrophicus*-like sequence (nonphotosynthetic bacterium that contains bacteriochlorophyll *a*), and the Dante sample contained one *Cyanobacteria* sequence (aerobic, oxygenic photosynthetic bacteria) thus supporting the detection of chlorophyll in these samples. No chlorophyll or other photosynthetic pigments or chlorophyll-containing bacteria were found in the Hot Harold sample. The chlorophyll spectra match a bacterial mat spectrum from an anoxic mat in pyrite-rich sediments growing 34 m deep in an Antarctic lake below 3 m of ice [*Bishop et al.*, 2001]. The green photosynthetic bacteria in Bastille are anaerobes, consistent with the other organisms found in the sample, and may be growing chemosynthetically on H_2 and sulfur compounds, but possess some basal level of photosynthetic pigments. Anaerobic, photosynthetic green sulfur bacteria were previously isolated from a deep-sea black smoker from the East Pacific Rise [*Beatty et al.*, 2005]. Further development of spectral libraries from appropriate diverse chimney types would greatly improve their accuracies for this application, which shows great potential.

These spectroscopic techniques show enormous promise for shipboard analyses. Shipboard measurement of the VNIR spectra could provide fast and nondestructive analysis for minerals and photosynthetic pigments to ensure that the samples collected represent the desired communities. The widespread availability of portable reflectance spectrometers opens the possibility of obtaining shipboard fine-scale characterization of samples that may provide a better understanding of microbe-mineral interactions within active hydrothermal chimneys. In the future, shipboard analyses can also be acquired with hyperspectral imaging, providing an understanding of the spatial distribution of major phases present at smaller than centimeter-scale resolution. These rapid analyses may serve as important guides for coregistered sampling strategies that delineate different mineralogical and biological zones, hence leading to more representative characterization of mineral-microbial habitats.

5.2. Comparison of Microbial Community Composition and Calculated Reaction Energetics

The chimney from the Bastille edifice contained primarily mesophilic, thermophilic, and hyperthermophilic anaerobes, and mostly heterotrophic sulfate reducers of the *Deltaproteobacteria*. The chimneys from the Dante and Hot Harold edifices contained microbial communities that were similar to each other and composed primarily of mesophilic and thermophilic aerobes, mostly *Betaproteobacteria* and *Epsilonproteobacteria*, although an equal proportion of *Epsilonproteobacteria* was also present in the Bastille chimney. The autotrophs in these later samples were primarily aerobic sulfide oxidizers. The mixed seawater-hydrothermal fluid in all three chimneys was calculated to be oxygenic at all microbial growth temperatures, although the temperature of the transition from oxygenated to anoxic conditions was lower for the Bastille fluid (101°C) than for the other two mixed fluids (117 and 202°C). Oxygenation of the mixed fluids is more pronounced, and H_2 is absent at microbial growth temperatures, when H_2 and O_2 are modeled in equilibrium and mineral precipitation is inhibited demonstrating that these assumptions are not adequate for this system. The difference observed in the Bastille microbial community composition, despite close similarities in fluid chemistry for all three samples, indicates that additional factors influence the types of microbes and microbial processes present within a chimney.

The thermodynamic energy available for microbial redox reactions in hydrothermal systems has been calculated for batch mixtures of hydrothermal fluid and seawater [*Amend et al.*, 2011; *Dahle et al.*, 2015; *McCollom and Shock*, 1997] and by considering diffusive and advective transport of heat and mass in vent structures [*Tivey*, 2004]. These include hydrothermal fluids from the MEF at Endeavour [*Amend et al.*, 2011; *Tivey*, 2004]. The calculated conditions, particularly the pH and the oxidation state of the pore fluid within hydrothermal chimneys, differ significantly when conductive cooling of hydrothermal fluid, diffusion, and advection of hydrothermal fluid out of the structure are considered relative to batch mixing of vent fluid and seawater in the chimney [*Tivey*, 2004]. The transition temperature from oxygenated to anoxic conditions is much lower when the flow of seawater into a chimney structure is limited (i.e., conductive cooling, diffusion only, advection of vent fluid out of the structure), which could explain the predominantly anaerobic microbial community in the Bastille sample. However, conductive cooling, diffusion, and advection of hydrothermal fluid out of a structure also lead to very low pH conditions (<pH 3–4) in the fluids at temperatures below 120°C while batch mixing and advection of seawater into the structure raises the pH (>pH 4.5) at these temperatures [*Tivey*, 2004]. Nearly all of the 16S rRNA gene sequences from all three samples were most closely related to microorganisms that grow at slightly acidic (>pH 5) to neutral pH conditions (supporting information Table S2), which supports the idea of seawater advection into the chimney and mixing of seawater and hydrothermal fluid. The general pattern of redox reaction energy availability calculated in this study was the same as those reported previously with aerobic sulfide and methane oxidation being nearly equal (up to 19–22 J/kg and 22–25 J/kg, respectively) and significantly higher than all other reactions (up to 5 J/kg for aerobic hydrogen oxidation, <1 J/kg for sulfate reduction, methanogenesis, and anaerobic oxidation of methane) [*Amend et al.*, 2011; *Tivey*, 2004]. These previous predictions and those herein largely match the community compositions observed in the Dante and Hot Harold chimneys. The amounts of energy available for aerobic respiration and hydrogenotrophic sulfate reduction and methanogenesis at Endeavour were much lower in this study relative to previous studies due to significantly lower O_2 and H_2 concentrations herein.

The predominance of anaerobes in the Bastille sample indicates that there were other means of creating anoxic conditions within the chimney at microbial growth temperatures that were not accounted for in the mixing model. Possible explanations include aqueous abiotic Fe^{2+} and S^{2-} oxidation, weathering of reduced minerals by seawater ingress, and depletion of O_2 by aerobic respiration. Aqueous Fe^{2+} concentrations were highest in Bastille fluids and predicted to lower the oxic-anoxic interface temperature relative to the other two chimney fluids. Pyrite is oxidized by Fe^{3+}, which adsorbs to the pyrite and forms Fe^{2+} and SO_4^{2-}, and by O_2, but the reaction rate is 10-fold slower than Fe^{3+} as an oxidant [*Luther*, 1987; *Moses et al.*, 1987]. However, there was no textural evidence of seawater-induced mineral oxidation by petrography. Alternatively, the dense macrofauna and bacterial mat on the exterior of the Bastille chimney and the heterotrophic microbes in the interior may consume the O_2 flowing into the interior of the chimney. The exterior biomass could also provide the organic compounds for the largely heterotrophic microbial population found in the midwall section of the chimney. Molecular and culture-based analyses suggest that most of the hyperthermophiles found in the midwall section of Bastille are heterotrophs with minor

hydrogenotrophs such as methanogens. The predicted H_2 concentration in mixed Bastille fluid at 80°C is $\sim$8 μmol kg^{-1}, which is below the minimum H_2 threshold needed to support the growth of *Methanocaldococcus* species [*Ver Eecke et al.*, 2012], which were the closest relatives to the Bastille 16S rRNA gene sequences. However, hyperthermophilic heterotrophs such as *Thermococcus* species, which were the closest relatives to sequences in Bastille, have been shown to support the growth of methanogens through H_2 syntrophy [*Ver Eecke et al.*, 2012]. Therefore, the ingress of organic compounds from the exterior of the Bastille chimney may also indirectly support the growth of hydrogenotrophs through H_2 syntrophy.

The aerobic autotrophs in the Bastille, Dante, and Hot Harold chimneys are largely dependent upon the aqueous chemical species in hydrothermal fluids, such as H_2S, and O_2 in seawater for their growth. The presence and predominance of *Betaproteobacteria* in the Dante and Hot Harold chimneys is unusual; however, they have been found in other molecular analyses from the Endeavour Segment [*Anderson et al.*, 2013; *Zhou et al.*, 2009]. The *Betaproteobacteria* in this study show some distant similarity to known metal oxidizing bacteria such as *Leptothrix* and heavy metal tolerant bacteria such as *Cupriavidus* and may have similar functions [*Goris et al.*, 2001]. However, while our controls were negative, we also cannot rule out the possibility that our high homology ($>$99% identity) *Betaproteobacteria* are contaminants in these samples with low DNA concentrations, as previously observed [*Zeigler Allen et al.*, 2011].

Few studies have correlated microbial community composition and rates of microbial activity with hydrothermal chimney mineralogy, and fewer studies also examined fluid chemistry composition. Combined chimney mineralogy and microbial community composition were examined at Endeavour using a chimney from the Mothra hydrothermal field that was venting 302°C fluid and a chimney from the Main Endeavour Field that was venting 330°C fluid [*Schrenk et al.*, 2003; *Zhou et al.*, 2009]. Neither study examined hydrothermal fluid chemistry. Both chimneys had a chalcopyrite-lined central fluid conduit with wurtzite, sphalerite, and pyrite in the midwall sections of the chimneys suggesting that they were mature Type I chimneys. As in our study, the interior midwall sections of these chimneys contained anaerobic hyperthermophilic archaea. *Zhou et al.* [2009] also examine the bacterial community and found that most were *Epsilonproteobacteria* most closely related to *Sulfurovum* and *Sulfurimonas* species. The results for these chimneys generally corroborate with our results for the Bastille chimney. Three predominantly anhydrite chimneys venting 123–261°C fluids were examined for anaerobic microbes from the Middle Valley hydrothermal vent field, also on the Endeavour Segment 70 km north of the Endeavour hydrothermal fields [*Frank et al.*, 2013; *Olins et al.*, 2013]. Anaerobic carbon fixation and sulfate reduction activities were measured in each of the chimneys, and anaerobes such as the thermophilic sulfate reducer *Thermodesulfovibrio* and hyperthermophiles belong to the *Archaeoglobi*, the *Thermoprotei* and the *Thermococci* were detected in molecular sequence analyses. Although the relative proportions of aerobes and anaerobes were not explicitly determined for these samples, the presence of anaerobes in predominantly anhydrite chimneys, which were also observed as minor components in the Dante and Hot Harold chimneys in this study, demonstrates that it is ultimately the fluid chemistry, fluid flow characteristics, and the chimney maturity, and not simply the mineralogy, that dictates the microbial community composition. However, both the minerals and microbes found in chimneys are influenced by these environmental conditions. In all hydrothermal chimneys, microscale heterogeneity is also likely an important factor that affects microbial community composition and activity [*Frank et al.*, 2013; *Olins et al.*, 2013] and should be an integral part of future studies.

6. Conclusions

The focus of this study was characterization of the mineralogy, fluid geochemistry, and microbiology of habitable zones in the interiors of active hydrothermal chimneys. Several studies have examined the microbial community composition in diffuse hydrothermal vent fluids along the Juan de Fuca Ridge [*Akerman et al.*, 2013; *Anderson et al.*, 2013; *Huber et al.*, 2002, 2003, 2007; *Meyers et al.*, 2013; *Opatkiewicz et al.*, 2009; *Ver Eecke et al.*, 2012]. Only a few studies have correlated microbial community compositions with the mineralogy of actively venting chimneys from the Juan de Fuca Ridge [*Olins et al.*, 2013; *Schrenk et al.*, 2003; *Zhou et al.*, 2009]. This study combined for the first time detailed mineralogy, fluid chemistry, redox reaction energetics, molecular microbial community analyses, and culture-dependent estimates of hyperthermophiles of active chimneys from the Endeavour Segment to assess the nature of their habitable interior zones. The results suggest that other factors, such as fluid flow characteristics, mineral composition and possible

weathering, and external aerobic respiration, may combine with fluid chemical composition to influence the kinds of minerals and microbial metabolisms present within a hydrothermal chimney. It also demonstrates that reflection and emission spectroscopy is a powerful tool for identifying minerals and microbial pigments in chimneys that could be used at sea for rapid selection of samples that can provide further insight into microbe-mineral-fluid chemistry interactions.

This study brings together diverse perspectives of marine geoscience, microbiology, mineral spectroscopy, and geochemistry to directly understand the nature and limits of life in hydrothermal chimneys. Hydrothermal vents are among the most productive regions in the deep ocean and represent an ideal starting point for modeling life in the ocean crust. With this study, we are not at the point of suggesting that mineralogy directly shapes microbial community composition. Rather environmental conditions within a chimney, shaped by chemistry, fluid flow, and other possible factors such as aerobic respiration of the O_2 in seawater during ingress and abiotic oxidation of Fe^{2+} and S^{2-}, can lead to the conditions that result both in a particular mineralogy and microbial community composition. The mineralogy may indirectly shape the community composition by affecting these other factors. While many questions remain to be addressed, a holistic approach that includes mineralogy, microbiology, and geochemistry will lead to a broader understanding and detection of life within rock.

References

Akerman, N. H., D. A. Butterfield, and J. A. Huber (2013), Phylogenetic diversity and functional gene patterns of sulfur-oxidizing subseafloor Epsilonproteobacteria in diffuse hydrothermal vent fluids, *Frontiers Microbiol.*, *4*, 185.

Amend, J. P., and E. L. Shock (2001), Energetics of overall metabolic reactions of thermophilic and hyperthermophilic Archaea and Bacteria, *FEMS Microbiol. Rev.*, *25*, 175–243.

Amend, J. P., T. M. McCollom, M. Hentscher, and W. Bach (2011), Catabolic and anabolic energy for chemolithoautotrophs in deep-sea hydrothermal systems hosted in different rock types, *Geochim. Cosmochim. Acta*, *75*, 5736–5748.

Anderson, R. E., M. T. Beltrán, S. J. Hallam, and J. A. Baross (2013), Microbial community structure across fluid gradients in the Juan de Fuca Ridge hydrothermal system, *FEMS Microbiol. Ecol.*, *83*, 324–339.

Bak, F., and F. Widdel (1986), Anaerobic degradation of indolic compounds by sulfate-reducing enrichment cultures, and description of *Desulfobacterium indolicum* gen. nov., sp. nov., *Arch. Microbiol.*, *146*, 170–176.

Beatty, J. T., J. Overmann, M. T. Lince, A. K. Manske, A. S. Lang, R. E. Blankenship, C. L. Van Dover, T. A. Martinson, and F. G. Plumley (2005), An obligately photosynthetic bacterial anaerobe from a deep-sea hydrothermal vent, *Proc. Natl. Acad. Sci. U. S. A.*, *102*, 9306–9310.

Bishop, J. L., A. Lougear, J. Newton, P. T. Doran, H. Froeschl, A. X. Trautwein, W. Körner, and C. Koeberl (2001), Mineralogical and geochemical analyses of Antarctic sediments: A reflectance and Mössbauer spectroscopy study with applications for remote sensing on Mars, *Geochim. Cosmochim. Acta*, *65*, 2875–2897.

Bishop, J. L., M. D. Lane, M. D. Dyar, and A. J. Brown (2008), Reflectance and emission spectroscopy study of four groups of phyllosilicates: Smectites, kaolinite-serpentines, chlorites and micas, *Clay Miner.*, *43*, 35–54.

Bishop, J. L., M. D. Lane, M. D. Dyar, S. J. King, A. J. Brown, and G. Swayze (2014), Spectral properties of Ca-sulfates: Gypsum, bassanite and anhydrite, *Am. Mineral.*, *99*, 2105–2115.

Bohnenstiehl, D. R., R. P. Dziak, M. Tolstoy, C. G. Fox, and M. Fowler (2004), Temporal and spatial history of the 1999–2000 Endeavour Segment seismic series, Juan de Fuca Ridge, *Geochem. Geophys. Geosyst.*, *5*, Q09003, doi:10.1029/2004GC000735.

Burns, R. (1993), *Mineralogical Applications of Crystal Field Theory*, 2nd ed., 551 pp., Cambridge Univ. Press, Cambridge, U. K.

Butterfield, D. A., R. E. McDuff, M. J. Mottl, M. D. Lilley, J. E. Lupton, and G. J. Massoth (1994), Gradients in the composition of hydrothermal fluids from the Endeavour segment vent field: Phase separation and brine loss, *J. Geophys. Res.*, *99*, 9561–9583.

Butterfield, D. A., I. R. Jonasson, G. J. Massoth, R. A. Feely, K. K. Roe, R. E. Embley, J. F. Holden, R. E. McDuff, M. D. Lilley, and J. R. Delaney (1997), Seafloor eruptions and evolution of hydrothermal fluid chemistry, *Philos. Trans. R. Soc. London A*, *355*, 369–386.

Caporaso, J. G., et al. (2010), QIIME allows analysis of high-throughput community sequencing data, *Nat. Methods*, *7*, 335–336.

Carbotte, S. M., J. P. Canales, M. R. Nedimovic, H. Carton, and J. C. Mutter (2012), Recent seismic studies at the East Pacific Rise 8°20′–10°10′ N and Endeavour Segment: Insights into mid-ocean ridge hydrothermal and magmatic processes, *Oceanography*, *25*, 100–112.

Clague, D. A., D. W. Caress, H. Thomas, D. Thompson, M. Calarco, J. Holden, and D. Butterfield (2008), Abundance and distribution of hydrothermal chimneys and mounds on the Endeavour Ridge determined by 1-m resolution AUV multibeam mapping surveys, *Eos Trans. AGU*, *89*(53), Fall Meet. Suppl., Abstract V41B-2079.

Clague, D. A., et al. (2014), Eruptive and tectonic history of the Endeavour Segment, Juan de Fuca Ridge, based on AUV mapping data and lava flow ages, *Geochem. Geophys. Geosyst.*, *15*, 3364–3391, doi:10.1002/2014GC005415.

Clark, R. N., G. A. Swayze, R. Wise, E. Livo, T. Hoefen, R. Kokaly, and S. J. Sutley (2007), *USGS Digital Spectral Library splib06a, Digital Data Ser.*, vol. 231, U.S. Geol. Surv., Flagstaff, Ariz. [Available at http://speclab.cr.usgs.gov/spectral.lib06/.]

Dahle, H., I. Økland, I. H. Thorseth, R. B. Pederesen, and I. H. Steen (2015), Energy landscapes shape microbial communities in hydrothermal systems on the Arctic Mid-Ocean Ridge, *ISME J.*, *9*, 1593–1606.

Davis, E. E., K. Wang, R. E. Thomson, K. Becker, and J. F. Cassidy (2001), An episode of seafloor spreading and associated plate deformation inferred from crustal fluid pressure transients, *J. Geophys. Res.*, *106*, 21,953–21,963.

Delaney, J. R., V. Robigou, R. E. McDuff, and M. K. Tivey (1992), Geology of a vigorous hydrothermal system on the Endeavour Segment, Juan de Fuca Ridge, *J. Geophys. Res.*, *97*, 19,663–19,682.

DeSantis, T. Z., et al. (2006), Greengenes, a chimera-checked 16S rRNA gene database and workbench compatible with ARB, *Appl. Environ. Microbiol.*, *72*, 5069–5072.

Edgar, R. C. (2010), Search and clustering orders of magnitude faster than BLAST, *Bioinformatics*, *26*, 2460–2461.

Edgar, R. C., B. J. Haas, J. C. Clemente, C. Quince, and R. Knight (2011), UCHIME improves sensitivity and speed of chimera detection, *Bioinformatics*, *27*, 2194–2200.

Edmond, J. M., G. J. Massoth, and M. D. Lilley (1992), Submersible-deployed samplers for axial vent waters, *RIDGE Events*, *3*, 23–24.

Frank, K. L., D. R. Rogers, H. C. Olins, C. Vidoudez, and P. R. Girguis (2013), Characterizing the distribution and rates of microbial sulfate reduction at Middle Valley hydrothermal vents, *ISME J.*, *7*, 1391–1401.

Goldfarb, M. S., D. R. Converse, H. D. Holland, and J. M. Edmond (1983), The genesis of hot spring deposits on the East Pacific Rise, 21°N, *Econ. Geol. Monogr.*, *5*, 184–197.

Goris, J., P. De Vos, T. Coenye, B. Hoste, D. Janssens, H. Brim, L. Diels, M. Mergeay, K. Kersters, and P. Vandamme (2001), Classification of metal-resistant bacteria from industrial biotopes as *Ralstonia campinensis* sp. nov., *Ralstonia metallidurans* sp. nov. and *Ralstonia basilensis* Steinle *et al*. 1998 emend, *Int. J. Syst. Evol. Microbiol.*, *51*, 1773–1782.

Hafenbradl, D., M. Keller, R. Dirmeier, R. Rachel, P. Rossnagel, S. Burggraf, H. Huber, and K. O. Stetter (1996), *Ferroglobus placidus* gen. nov., sp. nov., a novel hyperthermophilic archaeum that oxidizes Fe^{2+} at neutral pH under anoxic conditions, *Arch. Microbiol.*, *166*, 308–314.

Hannington, M. D., I. R. Jonasson, P. M. Herzig, and S. Petersen (1995), Physical and chemical processes of seafloor mineralization at mid-ocean ridges, in *Seafloor Hydrothermal Systems: Physical, Chemical, Biological, and Geological Interactions*, vol. 91, edited by S. E. Humpries et al., pp. 115–157, AGU, Washington, D. C.

Haymon, R. (1983), Growth history of hydrothermal black smoker chimneys, *Nature*, *301*, 695–698.

Hedrick, D. B., R. D. Pledger, D. C. White, and J. A. Baross (1992), In situ microbial ecology of hydrothermal vent sediments, *FEMS Microbiol. Ecol.*, *101*, 1–10.

Hooft, E. E. E., et al. (2010), A seismic swarm and regional hydrothermal and hydrologic perturbations: The northern Endeavour Segment, February, 2005, *Geochem. Geophys. Geosyst.*, *11*, Q12015, doi:10.1029/2010GC003264.

Hubas, C., B. Jesus, C. Passarelli, and C. Jeanthon (2011), Tools providing new insight into coastal anoxygenic purple bacterial mats: Review and perspectives, *Res. Microbiol.*, *162*, 858–868.

Huber, J. A., D. A. Butterfield, and J. A. Baross (2002), Temporal changes in archaeal diversity and chemistry in a mid-ocean ridge subseafloor habitat, *Appl. Environ. Microbiol.*, *68*, 1585–1594.

Huber, J. A., D. A. Butterfield, and J. A. Baross (2003), Bacterial diversity in a subseafloor habitat following a deep-sea volcanic eruption, *FEMS Microbiol. Evol.*, *43*, 393–409.

Huber, J. A., D. B. Mark Welch, H. G. Morrison, S. M. Huse, P. R. Neal, D. A. Butterfield, and M. L. Sogin (2007), Microbial population structures in the deep marine biosphere, *Science*, *318*, 97–100.

Inagaki, F., K. Takai, H. Kobayashi, K. H. Nealson, and K. Horikoshi (2003), *Sulfurimonas autotrophica* gen. nov., sp. nov., a novel sulfur-oxidizing ε-protobacterium isolated from hydrothermal sediments in the Mid-Okinawa Trough, *Int. J. Syst. Evol. Microbiol.*, *53*, 1801–1805.

Itoh, T. (2003), Taxonomy of nonmethanogenic hyperthermophilic and related thermophilic archaea, *J. Biosci. Bioeng.*, *96*, 203–212.

Itoh, T., K. Suzuki, and T. Nakase (2002), *Vulcanisaeta distributa* gen. nov., sp. nov., and *Vulcanisaeta souniana* sp. nov., novel hyperthermophilic, rod-shaped crenarchaeotes isolated from hot springs in Japan, *Int. J. Syst. Evol. Microbiol.*, *52*, 1097–1104.

Jamieson, J. W., M. D. Hannington, D. A. Clague, D. S. Kelley, J. R. Delaney, J. F. Holden, M. K. Tivey, and L. E. Kimpe (2013), Sulfide geochronology along the Endeavour Segment of the Juan de Fuca Ridge, *Geochem. Geophys. Geosyst.*, *14*, 2084–2099, doi:10.1002/ggge.20133.

Jamieson, J. W., M. D. Hannington, and D. A. Clague (2014), Hydrothermal sulfide accumulation along the Endeavour Segment, Juan de Fuca Ridge, *Earth Planet. Sci. Lett.*, *395*, 136–148.

Jin, Q., and C. M. Bethke (2005), Predicting the rate of microbial respiration in geochemical environments, *Geochim. Cosmochim. Acta*, *69*, 1133–1143.

Karsten, J. L., S. R. Hammond, E. E. Davis, and R. G. Currie (1986), Detailed geomorphology and neotectonics of the Endeavour Segment, Juan de Fuca Ridge: New results from Seabeam swath mapping, *Geol. Soc. Am. Bull.*, *97*, 213–221.

Kashefi, K., D. E. Holmes, J. A. Baross, and D. R. Lovley (2003), Thermophily in the *Geobacteraceae*: *Geothermobacter ehrlichii* gen. nov., sp. nov., a novel thermophilic member of the *Geobacteraceae* from the "Bag City" hydrothermal vent, *Appl. Environ. Microbiol.*, *69*, 2985–2993.

Kelley, D. S., J. R. Delaney, and D. R. Yoerger (2001), Geology and venting characteristics of the Mothra hydrothermal field, Endeavour segment, Juan de Fuca Ridge, *Geology*, *29*, 959–962.

Kelley, D. S., J. A. Baross, and J. R. Delaney (2002), Volcanoes, fluids, and life at mid-ocean ridge spreading centers, *Annu. Rev. Earth Planet. Sci.*, *30*, 385–491.

Kelley, D. S., et al. (2012), Endeavour Segment of the Juan de Fuca Ridge: One of the most remarkable places on Earth, *Oceanography*, *25*, 44–61.

Kelley, D. S., J. R. Delaney, and S. K. Juniper (2014), Establishing a new era of submarine volcanic observatories: Cabling Axial Seamount and the Endeavour Segment of the Juan de Fuca Ridge, *Mar. Geol.*, *352*, 426–450.

Klima, R. L., C. M. Pieters, and M. D. Dyar (2007), Spectroscopy of synthetic Mg-Fe pyroxenes. I: Spin-allowed and spin-forbidden crystal field bands in the visible and near-infrared, *Meteorit. Planet. Sci.*, *42*, 235–253.

Kormas, K. A., M. K. Tivey, K. Von Damm, and A. Teske (2006), Bacterial and archaeal phylotypes associated with distinct mineralogical layers of a white smoker spire from a deep-sea hydrothermal vent site (9°N, East Pacific Rise), *Environ. Microbiol.*, *8*, 909–920.

Koski, R. A., I. R. Jonasson, D. C. Kadko, V. K. Smith, and F. L. Wong (1994), Compositions, growth mechanisms, and temporal relations of hydrothermal sulfide-sulfate-silica chimneys at the northern Cleft segment, Juan de Fuca Ridge, *J. Geophys. Res.*, *99*, 4813–4832.

Kristall, B., D. S. Kelley, M. D. Hannington, and J. R. Delaney (2006), Growth history of a diffusely venting sulfide structure from the Juan de Fuca Ridge: A petrological and geochemical study, *Geochem. Geophys. Geosyst.*, *7*, Q07001, doi:10.1029/2005GC001166.

Kristall, B., D. Nielsen, M. D. Hannington, D. S. Kelley, and J. R. Delaney (2011), Chemical microenvironments within sulfide structures from the Mothra Hydrothermal Field: Evidence from high-resolution zoning of trace elements, *Chem. Geol.*, *290*, 12–30.

Lane, M. D. (2007), Midinfrared emission spectroscopy of sulfate and sulfide-bearing minerals, *Am. Mineral.*, *92*, 1–18.

Lane, M. D. (2008), Sulfide minerals studied using thermal emission spectroscopy, in *Lunar and Planetary Science XXXIX*, Abstract #2205, Lunar and Planet. Inst., Houston, Tex.

Larkin, M., et al. (2007), ClustalW and ClustalX version 2.0, *Bioinformatics*, *23*, 2947–2948.

Lilley, M. D., D. A. Butterfield, E. J. Olson, J. E. Lupton, S. A. Macko, and R. E. McDuff (1993), Anomalous CH_4 and NH_4^+ concentrations at an unsedimented mid-ocean-ridge hydrothermal system, *Nature*, *364*, 45–47.

Lilley, M. D., D. A. Butterfield, J. E. Lupton, and E. J. Olson (2003), Magmatic events can produce rapid changes in hydrothermal vent chemistry, *Nature*, *422*, 878–881.

Lozupone, C., and R. Knight (2005), UniFrac: A new phylogenetic method for comparing microbial communities, *Appl. Environ. Microbiol.*, *71*, 8228–8235.

Luther, G. W., III (1987), Pyrite oxidation and reduction: Molecular orbital theory considerations, *Geochim. Cosmochim. Acta*, *51*, 3193–3199.

McCollom, T. M., and E. L. Shock (1997), Geochemical constraints on chemolithoautotrophic metabolism by microorganisms in seafloor hydrothermal systems, *Geochim. Cosmochim. Acta*, *61*, 4375–4391.

McDonald, D., M. N. Price, J. Goodrich, E. P. Nawrocki, T. Z. DeSantis, A. Probst, G. L. Andersen, R. Knight, and P. Hugenholtz (2012), An improved Greengenes taxonomy with explicit ranks for ecological and evolutionary analyses of bacteria and archaea, *ISME J.*, *6*, 610–618.

Meyer, J. L., N. H. Akerman, G. Proskurowski, and J. A. Huber (2013), Microbiological characterization of post-eruption "snowblower" vents at Axial Seamount, Juan de Fuca Ridge, *Frontiers Microbiol.*, *4*, 153.

Mills, R. A., and H. Elderfield (1995), Rare earth element geochemistry of hydrothermal deposits from the active TAG Mound, 26°N Mid-Atlantic Ridge, *Geochim. Cosmochim. Acta*, *59*, 3511–3524.

Moses, C. O., D. K. Nordstrom, J. S. Herman, and A. L. Mills (1987), Aqueous pyrite oxidation by dissolved oxygen and by ferric iron, *Geochim. Cosmochim. Acta*, *51*, 1561–1571.

Olins, H. C., D. R. Rogers, K. L. Frank, C. Vidoudez, and P. R. Girguis (2013), Assessing the influence of physical, geochemical and biological factors on anaerobic microbial primary productivity within hydrothermal vent chimneys, *Geobiology*, *11*, 279–293.

Opatkiewicz, A. D., D. A. Butterfield, and J. A. Baross (2009), Individual hydrothermal vents at Axial Seamount harbor distinct subseafloor microbial communities, *FEMS Microbiol. Ecol.*, *70*, 413–424.

Pagé, A., M. K. Tivey, D. S. Stakes, and A.-L. Reysenbach (2008), Temporal and spatial archaeal colonization of hydrothermal vent deposits, *Environ. Microbiol.*, *10*, 874–884.

Pierson, B. K., A. Oesterle, and G. L. Murphy (1987), Pigments, light penetration, and photosynthetic activity in the multi-layered microbial mats of Great Sippewissett Salt Marsh, Massachusetts, *FEMS Microbiol. Ecol.*, *45*, 365–376.

Pieters, C. M. (1983), Strength of mineral absorption features in the transmitted component of near-infrared reflected light: First results from RELAB, *J. Geophys. Res.*, *88*, 9534–9544.

Proskurowski, G., M. D. Lilley, and T. A. Brown (2004), Isotopic evidence of magmatism and seawater bicarbonate removal at the Endeavour hydrothermal system, *Earth Planet. Sci. Lett.*, *225*, 53–61.

Reysenbach, A.-L., Y. Liu, A. B. Banta, T. J. Beveridge, J. D. Kirshtein, S. Schouten, M. K. Tivey, K. L. Von Damm, and M. A. Voytek (2006), A ubiquitous thermoacidophilic archaeon from deep-sea hydrothermal vents, *Nature*, *442*, 444–447.

Robigou, V., J. R. Delaney, and D. S. Stakes (1993), Large massive sulfide deposits in a newly discovered active hydrothermal system, the High-Rise Field, Endeavour Segment, Juan de Fuca Ridge, *Geophys. Res. Lett.*, *20*, 1887–1890.

Ruff, S. W., P. R. Christensen, P. W. Barbera, and D. L. Anderson (1997), Quantitative thermal emission spectroscopy of minerals: A laboratory technique for measurement and calibration, *J. Geophys. Res.*, *102*, 14,899–14,913.

Sass, A., H. Rütters, H. Cypionka, and H. Sass (2002), *Desulfobulbus mediterraneus* sp. nov., a sulfate-reducing bacterium growing on mono- and disaccharides, *Arch. Microbiol.*, *177*, 468–474.

Schloss, P. D., et al. (2009), Introducing Mothur: Open-source, platform-independent, community-supported software for describing and comparing microbial communities, *Appl. Environ. Microbiol.*, *75*, 7537–7541.

Schnell, S., F. Bak, and N. Pfennig (1989), Anaerobic degradation of aniline and dihydroxybenzenes by newly isolated sulfate-reducing bacteria and description of *Desulfobacterium aniline*, *Arch. Microbiol.*, *152*, 556–563.

Schrenk, M. O., D. S. Kelley, J. R. Delaney, and J. A. Baross (2003), Incidence and diversity of microorganisms within the walls of an active deep-sea sulfide chimney, *Appl. Environ. Microbiol.*, *69*, 3580–3592.

Seewald, J., A. Cruse, and P. Saccocia (2003), Aqueous volatiles in hydrothermal fluids from the Main Endeavour Field, northern Juan de Fuca Ridge: Temporal variability following earthquake activity, *Earth Planet. Sci. Lett.*, *216*, 575–590.

Seyfried, W. E., J. S. Seewald, M. E. Berndt, K. Ding, and D. I. Foustoukos (2003), Chemistry of hydrothermal fluids from the Main Endeavour Field, northern Juan de Fuca Ridge: Geochemical controls in the aftermath of June 1999 seismic events, *J. Geophys. Res.*, *108*(B9), 2429, doi:10.1029/2002JB001957.

Slobodkina, G. B., T. V. Kolganova, J. Querellou, E. A. Bonch-Osmolovskaya, and A. I. Slobodkin (2009), *Geoglobus acetivorans* sp. nov., an iron(III)-reducing archaeon from a deep-sea hydrothermal vent, *Int. J. Syst. Evol. Microbiol.*, *59*, 2880–2883.

Takai, K., T. Komatsu, F. Inagaki, and K. Horikoshi (2001), Distribution of archaea in a black smoker chimney structure, *Appl. Environ. Microbiol.*, *67*, 3618–3629.

Takai, K., M. Suzuki, S. Nakagawa, M. Miyazaki, Y. Suzuki, F. Inagaki, and K. Horikoshi (2006), *Sulfurimonas paralvinellae* sp. nov., a novel mesophilic, hydrogen- and sulfur-oxidizing chemolithoautotroph within the *Epsilonproteobacteria* isolated from a deep-sea hydrothermal vent polychaete nest, reclassification of *Thiomicrospira denitrificans* as *Sulfurimonas denitrificans* comb. nov. and emended description of the genus *Sulfurimonas*, *Int. J. Syst. Evol. Microbiol.*, *56*, 1725–1733.

Thompson, J. R., L. A. Marcelino, and M. F. Polz (2002), Heteroduplexes in mixed-template amplifications: Formation consequence and elimination by "reconditioning PCR," *Nucleic Acids Res.*, *30*, 2083–2088.

Tivey, M. K. (1995), The influence of hydrothermal fluid composition and advection rates on black smoker chimney mineralogy: Insights from modeling transport and reaction, *Geochim. Cosmochim. Acta*, *59*, 1933–1949.

Tivey, M. K. (2004), Environmental conditions within active seafloor vent structures: Sensitivity to vent fluid composition and fluid flow, in *The Subseafloor Biosphere at Mid-Ocean Ridges vol. 144*, edited by W. S. D. Wilcock et al., pp. 137–152, AGU, Washington, D. C.

Tivey, M. K., and J. R. Delaney (1986), Growth of large sulfide structures on the Endeavour Segment of the Juan de Fuca Ridge, *Earth Planet. Sci. Lett.*, *77*, 303–317.

Tivey, M. K., and S. Singh (1997), Nondestructive imaging of fragile sea-floor vent deposit samples, *Geology*, *25*, 931–934.

Tivey, M. K., D. S. Stakes, T. L. Cook, M. D. Hannington, and S. Petersen (1999), A model for growth of steep-sided vent structures on the Endeavour Segment of the Juan de Fuca Ridge: Results of a petrologic and geochemical study, *J. Geophys. Res.*, *104*, 22,859–22,883.

Van Ark, E. M., R. S. Detrick, J. P. Canales, S. M. Carbotte, J. J. Harding, G. M. Kent, M. R. Nedimovic, W. S. D. Wilcock, J. B. Diebold, and J. M. Babcock (2007), Seismic structure of the Endeavour Segment, Juan de Fuca Ridge: Correlations with seismicity and hydrothermal activity, *J. Geophys. Res.*, *112*, B02401, doi:10.1029/2005JB004210.

Ver Eecke, H. C., D. S. Kelley, and J. F. Holden (2009), Abundances of hyperthermophilic autotrophic Fe(III) oxide reducers and heterotrophs in hydrothermal sulfide chimneys of the northeastern Pacific Ocean, *Appl. Environ. Microbiol.*, *75*, 242–245.

Ver Eecke, H. C., D. A. Butterfield, J. A. Huber, M. D. Lilley, E. J. Olson, K. K. Roe, L. J. Evans, A. Y. Merkel, H. V. Cantin, and J. F. Holden (2012), Hydrogen-limited growth of hyperthermophilic methanogens at deep-sea hydrothermal vents, *Proc. Natl. Acad. Sci. U. S. A.*, *109*, 13,674–13,679.

Von Damm, K. L. (1995), Controls on the chemistry and temporal variability of seafloor hydrothermal fluids, in *Seafloor Hydrothermal Systems: Physical, Chemical, Biological, and Geological Interactions*, vol. 91, edited by S. E. Humphries et al., pp. 222–247, AGU, Washington, D. C.

Von Damm, K. L., S. E. Oosting, R. Kozlowski, L. G. Buttermore, D. C. Colodner, H. N. Edmonds, J. M. Edmond, and J. M. Grebmeir (1995), Evolution of East Pacific Rise hydrothermal vent fluids following a volcanic eruption, *Nature*, *375*, 47–50.

Wang, Q., G. M. Garrity, J. M. Tiedje, and J. R. Cole (2007), Naive Bayesian classifier for rapid assignment of rRNA sequences into the new bacterial taxonomy, *Appl. Environ. Microbiol.*, *73*, 5261–5267.

Weekly, R. T., W. S. D. Wilcock, E. E. E. Hooft, D. R. Toomey, P. R. McGill, and D. Stakes (2013), Termination of a 6-year ridge-spreading event observed using a seafloor seismic network on the Endeavour Segment, Juan de Fuca Ridge, *Geochem. Geophys. Geosyst.*, *14*, 1375–1398, doi:10.1002/ggge.20105.

Wen, A., M. Fegan, C. Hayward, S. Chakraborty, and L. I. Sly (1999), Phylogenetic relationships among members of the Comamonadaceae, and description of *Delftia acidovorans* (den Dooren de Jong 1926 and Tamaoka et al. 1987) gen. nov., comb. nov., *Int. J. Syst. Evol. Microbiol.*, *49*, 567–576.

Werner, J. J., O. Koren, P. Hugenholtz, T. Z. DeSantis, W. A. Walters, J. G. Caporaso, L. T. Angenent, R. Knight, and R. E. Ley (2012), Impact of training sets on classification of high-throughput bacterial 16S rRNA gene surveys, *ISME J.*, *6*, 94–103.

Whitman, W. B., and C. Jeanthon (2006), Methanococcales, *Prokaryotes*, *3*, 257–273.

Wilcock, W. S. D., E. E. E. Hooft, D. R. Toomey, P. R. McGill, A. H. Barclay, D. S. Stakes, and T. M. Ramirez (2009), The role of magma injection in localizing black-smoker activity, *Nat. Geosci.*, *2*, 509–513.

Yabuuchi, E., Y. Kosako, I. Yano, H. Hotta, and Y. Nishiuchi (1995), Transfer of two *Burkholderia* and an *Alcanigenes* species to *Ralstonia* gen. nov.: Proposal of *Ralstonia pickettii* (Ralston, Palleroni and Doudoroff 1973) comb. nov., *Ralstonia solanacearum* (Smith 1896) comb. nov. and *Ralstonia eutropha* (Davis 1969) comb. nov., *Microbiol. Immunol.*, *39*, 897–904.

Zeigler Allen, L., T. Ishoey, M. A. Novotny, J. S. McLean, R. S. Lasken, and S. J. Williamson (2011), Single virus genomics: A new tool for virus discovery, *PLoS ONE*, *6*, e17722.

Zhou, H., J. Li, X. Peng, J. Meng, F. Wang, and Y. Ai (2009), Microbial diversity of a sulfide black smoker in Main Endeavour hydrothermal vent field, Juan de Fuca Ridge, *J. Microbiol.*, *47*, 235–247.

Zhu, W., M. K. Tivey, H. Gittings, and P. R. Craddock (2007), Permeability-porosity relationships in seafloor vent deposits: Dependence on pore evolution processes, *J. Geophys. Res.*, *112*, B05208, doi:10.1029/2006JB004716.

Zillig, W., I. Holz, D. Janekovic, H.-P. Klenk, E. Imsel, J. Trent, S. Wunderl, V. H. Forjaz, R. Coutinho, and T. Ferreira (1990), *Hyperthermus butylicus*, a hyperthermophilic sulfur-reducing archaebacterium that ferments peptides, *J. Bacteriol.*, *172*, 3959–3965.